

RESEARCH

Open Access



Repurposing nitric oxide donating drugs in cancer therapy through immune modulation

Chung-Yen Li¹, Gangga Anuraga^{2,3}, Chih-Peng Chang^{1,4}, Tzu-Yang Weng¹, Hui-Ping Hsu⁵, Hoang Dang Khoa Ta², Pei-Fang Su⁶, Pin-Hsuan Chiu⁷, Shiang-Jie Yang¹, Feng-Wei Chen¹, Pei-Hsuan Ye⁸, Chih-Yang Wang^{2,9,10*} and Ming-Derg Lai^{1,8*}

Abstract

Background Nitric oxide-releasing drugs are used for cardiovascular diseases; however, their effects on the tumor immune microenvironment are less clear. Therefore, this study explored the impact of nitric oxide donors on tumor progression in immune-competent mice.

Methods The effects of three different nitric oxide-releasing compounds (SNAP, SNP, and ISMN) on tumor growth were studied in tumor-bearing mouse models. Three mouse tumor models were used: B16F1 melanoma and LL2 lung carcinoma in C57BL/6 mice, CT26 colon cancer in BALB/c mice, and LL2 lung carcinoma in NOD/SCID mice. After nitric oxide treatment, splenic cytokines and lymphocytes were analyzed by cytokine array and flow cytometry, and tumor-infiltrating lymphocytes in the TME were analyzed using flow cytometry and single-cell RNA sequencing.

Results Low doses of three exogenous nitric oxide donors inhibited tumor growth in two immunocompetent mouse models but not in NOD/SCID immunodeficient mice. Low-dose nitric oxide donors increase the levels of splenic cytokines IFN- γ and TNF- α but decrease the levels of cytokines IL-6 and IL-10, suggesting an alteration in Th2 cells. Nitric oxide donors increased the number of CD8⁺ T cells with activation gene signatures, as indicated by single-cell RNA sequencing. Flow cytometry analysis confirmed an increase in infiltrating CD8⁺ T cells and dendritic cells. The antitumor effect of nitric oxide donors was abolished by depletion of CD8⁺ T cells, indicating the requirement for CD8⁺ T cells. Tumor inhibition correlated with a decrease in a subtype of protumor macrophages and an increase in a subset of Arg1-positive macrophages expressing antitumor gene signatures. The increase in this subset of macrophages was confirmed by flow cytometry analysis. Finally, the combination of low-dose nitric oxide donor and cisplatin induced an additive cancer therapeutic effect in two immunocompetent animal models. The enhanced therapeutic effect was accompanied by an increase in the cells expressing the gene signature of NK cell.

Conclusions Low concentrations of exogenous nitric oxide donors inhibit tumor growth in vivo by regulating T cells and macrophages. CD8⁺ T cells are essential for antitumor effects. In addition, low-dose nitric oxide donors may be combined with chemotherapeutic drugs in cancer therapy in the future.

Keywords Cancer, Immune, Nitric oxide donor, SNAP, Single-cell RNA-seq, CD8⁺ cytotoxic T cells, Macrophages

*Correspondence:

Chih-Yang Wang

chihyang@tmu.edu.tw

Ming-Derg Lai

a1211207@mail.ncku.edu.tw

Full list of author information is available at the end of the article



© The Author(s) 2023. **Open Access** This article is licensed under a Creative Commons Attribution 4.0 International License, which permits use, sharing, adaptation, distribution and reproduction in any medium or format, as long as you give appropriate credit to the original author(s) and the source, provide a link to the Creative Commons licence, and indicate if changes were made. The images or other third party material in this article are included in the article's Creative Commons licence, unless indicated otherwise in a credit line to the material. If material is not included in the article's Creative Commons licence and your intended use is not permitted by statutory regulation or exceeds the permitted use, you will need to obtain permission directly from the copyright holder. To view a copy of this licence, visit <http://creativecommons.org/licenses/by/4.0/>. The Creative Commons Public Domain Dedication waiver (<http://creativecommons.org/publicdomain/zero/1.0/>) applies to the data made available in this article, unless otherwise stated in a credit line to the data.

Background

Cancer is controlled by unrestricted growth of tumor cells and the influence of their microenvironments, including angiogenesis and evading immune destruction [1]. Tumor-associated macrophages (TAMs) are the most abundant immune cells in the tumor microenvironment (TME), and abundant TAMs in the TME are associated with poor clinical outcomes [2, 3]. TAMs are generally classified into two groups, namely M1 macrophages and M2 macrophages. During initial carcinogenesis, M1-like polarized macrophages play a role in the elimination of more immunogenic cancer cells. As the tumor progresses, M2-like polarization of macrophages plays a protumorigenic role in the tumor microenvironment by stimulating angiogenesis, lymphangiogenesis, and cancer cell proliferation [4]. Although the M1-like/M2-like paradigm is useful, it may be too simplified. Transcriptomic analysis suggested that a broad spectrum of differentiated TAMs may exist in the tumor microenvironment.

The second most abundant immune cells in the tumor microenvironment are T cells, which act as orchestrators and effectors of immunity. CD8⁺ T cells are the most prominent antitumor cells in cancer, and CD4⁺ T cells play an important role in the maintenance and activation of the CD8⁺ T cell response [5]. CD4⁺ type 1 helper T (Th1) cells mediate the antitumor response by secreting several cytokines to activate CD8⁺ T cells, macrophages, and NK cells [4]. Interestingly, T-cell dysfunction in the tumor microenvironment shares many features with T-cell exhaustion observed in chronic viral infection [6]. Dysfunction of T cells is usually associated with high expression of inhibitory receptors and loss of the production of cytokines IFN γ , IL-2 and TNF α [7].

Nitric oxide (NO) is a common molecule that participates in many cellular functions, such as neurotransmission [8–10] and vasoconstriction [11]. Some nitric oxide donors, such as sodium nitroprusside (SNP) and isosorbide mononitrate (ISMN), have been used to control hypertension in the clinic [12]. In addition to easing hypertension, nitric oxide functions as a cancer regulator, and the role of NO in cancer is dose dependent. Abnormally high supra-physiological NO concentrations (80 μ M) increase reactive nitrogen oxide species (RNS) formation, ultimately leading to DNA damage and carcinogenesis [13]. In vitro experiments have suggested that nitric oxide has an inhibitory function on immune cells and endothelial cell activation [14]. Interestingly, high doses of NO donors are suppressive in the expression of adhesion molecules in endothelial cells. In contrast, lower physiological concentrations induce immune activation, and the effects are likely associated with the

regulation of adhesion molecules in an NF κ B-dependent pathway [15]. These pieces of evidence indicate that the dose of NO may determine whether NO is protumorigenic or antitumorigenic. Expression of inducible nitric oxide synthase (iNOS) protein from myeloid-derived suppression cells (MDSCs) interferes with CD8⁺ T cell-mediated anti-tumor response [16]. In contrast, iNOS-expressing M1 macrophages inhibits tumor progression via high level NO and secretion of pro-inflammatory cytokines [17]. Endogenous NO, produced by nitric oxide synthase, regulates tumor progression via the immune system in a dose-dependent fashion [18]. Fewer studies have been performed on the effects of exogenous NO on immune cells in TME. Delivery of nitric oxide with a nanocarrier inhibits tumor progression through vessel normalization and increase of infiltrated CD8⁺ T cells in the TME [19]. The polynitrosated polyesters-based NO nanogenerator (NanoNO) enhances immunogenic cell death and potentiates cancer immunotherapy to prevent metastasis [20].

Several nitric oxide-releasing drugs have been used for a long time to treat cardiovascular diseases, such as isosorbide mononitrate (ISMN), which is a long-term nitric oxide-releasing drug administered to patients with hypertension [21]. Patients need to take ISMN daily to control blood pressure [22]. Moreover, other nitric oxide-releasing drugs, such as nitroglycerin and SNP, are commonly used as short-acting anti-angina agents to quickly decrease blood pressure [23, 24]. Although these drugs are used in millions of patients every year, the effects of nitric oxide-releasing drugs on cancer progression and the immune system are less studied.

Given that the direct effects of nitric oxide-releasing drugs on tumor cells or endothelial cells have been studied in vivo, we aimed to investigate whether exogenous nitric oxide regulates tumor progression through immune regulation. In this report, we studied the effects of several nitric oxide-releasing compounds (including FDA-approved drugs) on tumor progression in immune-competent mouse models. Furthermore, cytokine analysis and single-cell RNA sequencing were used to analyze various populations of immune cells and transcriptome alterations after treatment with exogenous nitric oxide-releasing drugs.

Our results demonstrated that low-dose exogenous nitric oxide induced an antitumor effect via CD8⁺ T cells. Additionally, low-dose nitric oxide increased a subset of Arg1-positive macrophages expressing M1-related genes, which may be associated with the antitumor immune response. Finally, a combination of low-dose nitric oxide releasing drugs and cisplatin increased the therapeutic effect in two different tumor-bearing mouse models.

Materials and methods

Cell culture reagents

B16F1 murine melanoma cells, LL2 murine Lewis lung carcinoma cells and CT26 murine colon carcinoma cells were used in this study. The B16F1, LL2 and CT26 cell lines were a kind gift from Dr. Ming-Shi Chang, Dr. Chao-Liang Wu and Dr. Liang-Yi Hung, respectively. These cell lines have been validated by American Type Culture Collection (ATCC). B16F1, LL2 and CT26 cells were cultured in high glucose Dulbecco's modified Eagle medium (HG-DMEM) (Cat. No. SH30003.02; HyClone, Logan, UT, USA), low glucose Dulbecco's modified Eagle medium (LG-DMEM) (Cat. No. SH30002.02; HyClone, Logan, UT, USA), and RPMI-1640 (Cat. No. CC110-0500; GeneDireX, Taiwan), respectively. S-Nitroso-N-acetyl-DL-penicillamine (SNAP) (N3398-50MG) and sodium nitroprusside (SNP) (BP453) were purchased from Sigma-Aldrich (Darmstadt, Germany). Isosorbide-5-mononitrate (ISMN; Cat. No. HY-B0642) was purchased from MedChemExpress (NJ, USA). SNP and ISMN were dissolved in phosphate buffered saline (PBS) (10 mg/ml) and diluted in PBS for animal experiments. SNAP was dissolved in dimethyl sulfoxide (DMSO; Cat. No. 34943-2.5L; Honeywell-Fluka, Charlotte, NC, USA) and diluted in PBS. Briefly, 1 mg SNAP was dissolved in 100 μ l DMSO and diluted with 900 μ l PBS (1 mg/ml SNAP containing 10% DMSO as a stock concentration). SNAP (0.0004 mg/ml) containing 0.004% DMSO was used for 0.004 mg/kg SNAP treatment in animal experiments. The same concentration of DMSO-containing PBS was used as a control in the SNAP experiment *in vivo*. All media were supplemented with 10% fetal bovine serum (FBS, Cat. No. A6806-31, NQBB International Biological Corporation, Hong Kong), 100 U/ml penicillin, and 100 mg/ml streptomycin (Cat. No. SV30010; HyClone). Cells were maintained at 37 °C in a 5% CO₂ incubator.

Mouse tumor models

Six- to ten-week-old mice (C57BL/6, NOD-SCID and BALB/c) were obtained from the Laboratory Animal Center at National Cheng Kung University (Tainan, Taiwan). All study protocols involving mice were approved by the Animal Welfare Committee at National Cheng Kung University. To observe the effect of nitric oxide donors on tumor development, the mice were subcutaneously implanted with 2×10^5 LL2, B16F1, or CT26 cells in the right flank. LL2 and B16F1 tumor-bearing mice were treated on Days 11, 12, 13, 16, 17, 18, 21, 22, and 23 with a nitric oxide donor by intraperitoneal injection (i.p.) after tumor cell implantation. The

schedule involved injection for 3 consecutive days followed by no treatment for two days. CT26 tumor-bearing mice were treated with a nitric oxide donor starting at Day 8 after tumor implantation. The tumors were examined every 2-4 days by measuring the length (L) and width (W). The tumor volume (V) was calculated as $V = (\text{width} \times \text{width} \times \text{length} \times 0.52)$. Mice were sacrificed using CO₂ when the tumor volume exceeded 2500 mm³.

Total serum nitrite/nitrate measurement

Total serum nitrite and nitrate were measured using an OxiSelect In Vitro Nitric Oxide (Nitrite/Nitrate) Assay kit (STA-802, Cell BioLabs, San Diego, CA, U.S.A.). Blood was collected in a tube without anticoagulant coating by submandibular blood collection 5 min after NO drug injection, and the serum was isolated by centrifugation at 2000x g for 10 min. Before the total nitrite/nitrate measurement, the serum was filtered with a 10-kDa MWCO ultrafilter through centrifugation at 5000x g for 10 min to reduce interference from protein. Fifty microliters of serum was cocultured with nitrate reductase for 1 hour at room temperature to recover nitrate into nitrite, and the total nitrite was detected with Griess reagents as a colored azo dye product. The absorbance was measured at 570 nm using a microplate reader (Multiskan FC Microplate Photometer, Thermo Fisher Scientific, Waltham, MA, USA).

Single-cell suspension preparation

Splenocytes and tumor masses were isolated from LL2 tumor-bearing mice 20 days after tumor cell implantation. Tumor tissues were cut into 2-mm pieces and digested using collagenase A (1 mg/ml) (Cat. No: 10103586001; Roche, Basel, Switzerland) and DNase (100 U/ml) (Cat. No: 11284932001; Roche), and the cell suspensions were placed in a 37 °C shaker (150 rpm) for 60 min. Splenocytes were crushed directly into cell suspensions using wire mesh. The cell suspensions were treated with red blood cell lysis buffer on ice for 5 min to remove RBCs. After RBC lysis, the cell suspensions were washed twice with 2 ml of flow staining buffer (Cat. No: 554656; BD Pharmingen, San Diego, CA, U.S. and filtered through a 0.35- μ m cell strainer (BD Pharmingen).

CD326⁺ tumor cell and intratumoral CD8⁺ T lymphocyte isolation

A 1×10^7 single-cell suspension of tumor tissue from LL2 tumor-bearing mice was used for CD326⁺ tumor cell and CD8⁺ T-cell isolation. Briefly, CD326⁺ cells were

collected using a CD326-positive selection magnetic bead kit (Cat. No. 130-105-958; Miltenyi Biotec, Bergisch Gladbach, Germany) following the manufacturer's instructions. CD326-positive tumor cells were used for the analysis of surface calreticulin, and CD326-negative cells were further used for CD8⁺ T-cell isolation with a CD8a-negative selection magnetic bead kit (Cat. No. 130-104-075; Miltenyi Biotec). The purity of the enriched CD8a⁺ T cells was homogeneously lysed in TRIzol for total RNA isolation.

RNA extraction and quantitative real-time polymerase chain reaction (RT-qPCR)

Total RNA was extracted from tumor-infiltrating CD8⁺ T cells, which were isolated using a CD8a⁺ T-cell isolation kit using TRIzol (Cyrusbioscience, Taiwan). MMLV reverse transcriptase (Promega, Madison, WI, USA) was used for cDNA synthesis. RT-qPCR was performed with a StepOne system (Applied Biosystems, Foster City, CA, USA) and Fast SYBR-Green Master Mix (Thermo Fisher Scientific). Relative RNA expression was calculated using the $2^{-\Delta\Delta C_t}$ method and normalized to glyceraldehyde 3-phosphate dehydrogenase (GAPDH) expression. The following forward and reverse primers for beta-catenin (Ctnnb1), transcription factor 7 (Tcf7), and GAPDH were used for RT-qPCR: Ctnnb1 forward, GTT CGC CTT CAT TAT GGA CTG CC; Ctnnb1 reverse, ATA GCA CCC TGT TCC CGC AAA G; Tcf7 forward, CCT GCG GAT ATA GAC AGC ACT TC; Tcf7 reverse, TGT CCA GGT ACA CCA GAT CCC A; GAPDH forward, CAT CAC TGC CAC CCA GAA GAC TG; and GAPDH reverse, ATG CCA GTG AGC TTC CCG TTC AG. GAPDH served as an internal control.

Flow cytometry

To investigate the alterations in infiltrating immune cells in the tumor microenvironment, we collected a single-cell suspension of tumor tissue from LL2 tumor-bearing mice. All infiltrating immune cells were stained with Fc blocker (Cat. No. 553141; BD Pharmingen) for 15 min on ice to reduce the nonspecific binding of antibodies on cells. Infiltrating CD8⁺ T cells were stained with BV510 rat anti-mouse CD45 (Cat. No. 563891; BD Pharmingen) and APC rat anti-mouse CD8a (Cat. No. 553035; BD Pharmingen). Mature dendritic cells in the tumor microenvironment were stained with BV510 rat anti-mouse CD45, BV421 hamster anti-mouse CD11c (Cat. No. 562782; BD Pharmingen), and APC rat anti-mouse CD86 (Cat. No. 561964; BD Pharmingen). To identify the population of TAM1-1 in the tumor, BV510 rat anti-mouse CD45, Alexa-488 rat anti-mouse IL7R (Cat. No. 561533; BD Pharmingen), and PE rat anti-mouse

CD80 (Cat. No. 561955; BD Pharmingen) were used for surface staining; BV421 rat anti-mouse CD68 (Cat. No. 566389; BD Pharmingen), and PE-Cy7-conjugated Arg1 (Cat. No. 25-3697-82; eBioscience, Waltham, MA, USA) were used for intracellular staining via BD Cytofix/Cytoperm™ Plus Fixation/Permeabilization Kit (Cat. No. 555028; BD Pharmingen) according to the manufacturer's instructions.

To determine the change in Th2 cells in splenocytes after low-dose SNAP treatment, splenocytes were collected at Day 20 after LL2 tumor implantation. Th2 cells were stained with Fc block for 15 min on ice and identified using PerCP-Cy5.5 rat anti-mouse CD45 (Cat. No. 550994; BD Pharmingen), APC rat anti-mouse CD4 (Cat. No. 552051; BD Pharmingen), and FITC rat anti-mouse IL-4 (Cat. No. 11-7042-82; eBioscience™). To measure the surface calreticulin in CD326⁺ tumor cells, CD326⁺ cells were isolated from a single-cell suspension of tumor tissue and stained with rabbit anti-mouse calreticulin (Ab2907; Abcam, Cambridge, UK) for 30 min on ice and further stained with goat anti-rabbit Alexa-488 (Ab150077; Abcam) for 30 min on ice. A Beckman CytoFLEX instrument was used for flow cytometry.

Single-cell isolation and library preparation

Tumor tissues from LL2 tumor-bearing mice were cut into 2-mm pieces, and tumor tissues were prepared into a single-cell suspension with collagenase A (1 mg/kg) and type I DNase (100 U/ml). Next, red blood cells were removed with red blood cell lysis buffer, and the single-cell suspensions were resuspended in flow staining buffer. Finally, the cells were treated with an Fc blocker to reduce the nonspecific binding of the Fc receptor and antibodies. The cells were labeled with BD™ Abseq Ab-logos (CD4 and CD8; Cat. No. 940108 and Cat. No. 940345), BD™ sample tag (Cat. No. 633793), and rat anti-mouse BV510-CD45 and 7-AAD (Cat. No. 51-65875X; BD Pharmingen). A total of 5×10^5 live immune cells (CD45 positive and 7-AAD negative) were sorted and resuspended in sample buffer for single-cell capture. Live CD45⁺ immune cells were captured using a BD Rhapsody™ system and lysed. Briefly, cells (10,000 cells/group) were loaded into a cartridge, which had 200,000 wells for cell loading. Then, the cell-capture beads, which carried three different single-stranded DNA fragments to bind the DNA fragments of the sample tag, Abseq Ab-logos, and mRNA, were loaded into the well for cell binding. Nonbinding beads were removed from cartridge after washing with buffer. The cells captured by one bead were lysed, and mRNA was converted into cDNA by a Rhapsody™ cDNA Kit (Cat. No. 633773; BD Pharmingen). Three libraries were established: a sample tag library, an Abseq library, and a whole

transcriptome analysis (WTA) library. Briefly, a sample tag library was used to distinguish different samples. The Abseq library could easily identify specific immune cells for transcriptome analysis. The WTA library was used for gene expression analysis. Library construction was performed by the Molecular Diagnostics Group of the Department of Pathology, National Cheng Kung University Hospital, and the single-cell library was analyzed using the NovaSeq 6000 system by the Institute of Molecular and Genomic Medicine of the National Health Research Institute.

Bioinformatics and computational biology analyses

Raw read data were aligned to the mouse genome (GRCm38.p6, gencode M19), and the expression matrix and sample tag matrix were produced by Rhapsody WTA pipeline V1.9. The control group with 4538 cells and the low-dose SNAP group with 4853 cells were used for further analysis. The count matrix was analyzed by the “Seurat” package [25] (Version 4.0.5). Genes and cells were removed under two conditions: cells with less than 700 feature genes and one feature gene with expression in less than 100 cells. After cell removal, we obtained 6563 cells (control: 3387, low-dose SNAP: 3176) for further analysis. The Seurat function “normalize Data” was used to normalize the raw count data. Variable genes were identified using the “FindVariableFeature” function. Default parameters were used for the Seurat function. Clusters were identified using the “FindClusters” function, and the resolution was 0.5. The dimensions of the data were reduced through UMAP. The differentially expressed genes in each cluster were identified via the “FindMarkers” function. When needed, clusters were combined into one cluster using the “Subset” function. Biological process (BP) and Kyoto Encyclopedia of Genes and Genomes (KEGG) analyses were performed using the “ClusterProfiler” package. Additionally, gene set enrichment analysis (GSEA) was performed using the “fgsea” package in R. We selected two GSEA databases for our analysis: hallmark gene sets and ontology gene sets. Moreover, MetaCore software was used for pathway analysis of significant genes. The cluster annotations were established based on signature genes that were approved by previous studies [26, 27]. Highly expressed genes in CD8⁺ T cells were assessed using *f* tests, *t* tests, and *p* values < 0.05. A list of significantly differentially expressed genes was imported into Metacore software to construct signaling pathways. The significance cutoff point for enrichment of a pathway was a *p* value < 0.05.

Cytokine array

The spleen was isolated from LL2 tumor-bearing mice on the 20th day after tumor implantation. A single-cell

suspension of splenocytes was prepared as described previously. To stimulate the cytokines secretion, splenocytes (5×10^5) were cultured with LL2 lysate in 2 ml of RPMI 1640 medium at 37 °C for 24 h. The culture medium was collected by centrifugation at 1500 rpm for 5 min, and the supernatant was collected and stored at -80 °C until use. Mouse Cytokine Array Panel A (Cat. No. ARY006; R&D Systems, Minneapolis, MN, USA) was used to measure the levels of 40 cytokines. For cytokine analysis, a 1-ml sample was mixed with 15 μ l of reconstituted Mouse Cytokine Array Panel A Detection Antibody Cocktail for 1 hour at room temperature, and the mixture was added to the array membrane and incubated overnight at 4 °C. Then, the array membranes were incubated with 2 ml of streptavidin-HRP for 30 min at room temperature. The array membranes were exposed to X-ray film, and the expression levels of each cytokine were quantitated by ImageJ software (Development by Dr. Wayne Rasband; National Institutes of Health).

Depletion of CD8⁺ T cells

The T-cell depletion protocol was performed as previously described with minor modifications. Anti-CD8 (clone: 53-6.7, Cat. No. BE0004-1, Bio X Cell, Lebanon, NH, U.S. A) (200 μ g per mouse) or rat IgG2a isotype control antibody (clone: 2A3, Cat. No. BE0089; Bio X Cell) was intraperitoneally injected into mice on Days 10 and 15. Approximately 90% of CD8⁺ T cells were depleted, as determined by flow cytometry analysis.

Biotin switch assay of S-nitrosylation protein and western blotting

To measure nitric oxide-induced protein nitrosylation, THP-1 cells were treated with different doses of SNP for 30 min, and 1 mg/ml protein was used for detection of S-nitrosylation protein. Here, S-nitrosylation of proteins was performed using an S-nitrosylated protein detection assay kit based on the biotin switch method (1006518, Cayman) following the manufacturer’s instructions. Total biotinylated proteins were purified with streptavidin-agarose beads (Thermo Fisher Scientific) for 1 hour at room temperature. Purified proteins were detected by western blotting. Nonpurified proteins were used as the input control, and the level of total nitrosylation protein was measured.

The following antibodies were used for western blotting: anti-GAPDH (Cat. No. GTX100118; GeneTex, Hsinchu, Taiwan) and anti-Hsp90 (Cat. No. 610418; BD Pharmingen). Total nitrosylation proteins were detected using an avidin-HRP conjugated antibody. Nitrosylated proteins were detected by western blotting following standard protocols. Images were obtained utilizing a

BioSpectrum AC imaging system (UVP, CA, USA) following the manufacturer's instructions.

Immunohistochemistry

Tumor-bearing mice were sacrificed 2 days after the second treatment (20th day after the implantation of tumor cells), and tumor tissues were collected in optimal cutting temperature (OCT) compound. Tumor tissues were sliced at a thickness of 5 μm . The tissue was fixed with 3.7% paraformaldehyde, and endogenous peroxidase was inactivated with 3% H_2O_2 at room temperature. Angiogenesis was detected with anti-CD31 (1:200 dilution) (Clone: MEC13.3, Cat. No. 550274, BD Pharmingen) antibody. The level of angiogenesis was assessed at a magnification of 100 \times . Five randomly chosen fields per sample from each mouse were evaluated.

Statistical analysis

All statistical analyses were performed using GraphPad Prism 8. All statistical analyses of tumors were performed with two-way ANOVA. Statistical analysis of the percentage of immune cell populations derived from FACS analysis was performed with t tests. A p value < 0.05 was considered statistically significant.

Results

Low-dose nitric oxide donors induced an antitumor response in immune-competent tumor-bearing mouse models but not in immune-deficient mice

To investigate the effect of the NO donor S-nitroso-N-acetyl-DL-penicillamine (SNAP) on tumorigenesis in a mouse model, the murine Lewis lung carcinoma (LL2) tumor cell line was subcutaneously implanted in the right flank of C57BL/6 mice. Tumor-bearing mice were treated with a nitric oxide donor at various doses, and the treatment schedule is illustrated in Fig. 1A. High-dose SNAP (0.02 mg/kg) did not affect tumor progression in LL2 tumor-bearing mice (Fig. 1B). However, a low dose of SNAP (0.004 mg/kg) induced an antitumor response in LL2 tumor-bearing mice (Fig. 1C). The antitumor effect of low-dose SNAP was dose dependent. A 10-fold lower dose of SNAP (0.0004 mg/kg) did not affect tumor growth in LL2 tumor-bearing mice (Fig. 1D). In addition, low-dose SNAP treatment (0.004 mg/kg) also induced an antitumor response in the B16F1 melanoma orthotopic mouse model (Fig. 1E). The FDA-approved nitric oxide drug sodium nitroprusside (SNP) reduced tumor growth in the 0.1 mg/kg treatment group (Fig. 1F). Similarly, another FDA-approved nitric oxide donor drug, isosorbide-5-mononitrate (ISMN), inhibited tumor growth at the same low dose (0.004 mg/kg) in an LL2 tumor-bearing animal model (Fig. 1G). The results of three different nitric oxide donors indicated that a low

dose of exogenous nitric oxide inhibited tumor growth. We then determined whether a low dose of nitric oxide donor increased NO levels or nitrosylated proteins in vivo and in vitro. The concentration of NO in mouse serum was increased 5 min after 0.1 mg/kg SNP treatment (p value = 0.09 in Supplementary Fig. 1 A). Due to an increase in NO levels after treatment with the low-dose NO-donating drug SNP in vivo, we further tested whether low-dose SNAP affected protein nitrosylation in vitro. Therefore, THP-1 monocytic cells were treated with increasing doses of SNAP, and protein nitrosylation was determined with an S-nitrosylated protein detection kit based on the biotin-switch method [28]. SNAP enhanced levels of total nitrosylated protein in THP-1 cells even at the very low concentration of 1 μM (Supplementary Fig. 1 B). Additionally, low-dose SNAP also enhanced the nitrosylation of heat-shock protein 90 (Hsp90), which is a known target of S-nitrosylation by NO [29] (Supplementary Fig. 1 C).

We next examined whether immune modulation was essential in mediating the antitumor response induced by low-dose SNAP and ISMN. LL2 tumor cells were implanted in the right flank of immune-deficient mice (NOD-SCID), and the therapeutic effects of low-dose SNAP and ISMN (0.004 mg/kg) were monitored. Low-dose SNAP and ISMN (0.004 mg/kg) did not affect tumor growth (Fig. 1H and I). Therefore, the immune system was essential for the low-dose SNAP-mediated antitumor response.

Low-dose SNAP regulated splenic cytokines and the Th2 cell population

Systemic immune activation is important for the response to immunotherapy [30], and we determined whether cytokines were regulated by low-dose SNAP treatment. Cytokine expression levels were analyzed using a cytokine array. We isolated tumor tissues and splenocytes on Day 20 after tumor implantation. Tumor weight and tumor size were reduced (Supplementary Fig. 2 A) in the low-dose SNAP (0.004 mg/kg) treatment group. To stimulate cytokine secretion, we cocultured LL2 cell lysates with splenocytes for 24 hours, and the supernatants were collected for cytokine detection using a cytokine array. The cytokines IL-6 and IL-10 are important for Th2-mediated function in cancer progression and exhibited reduced levels in the low-dose SNAP treatment group. Additionally, the levels of the cytokines IFN- γ and TNF- α were higher in the low-dose SNAP treatment group compared with in the control group (Supplementary Fig. 2 B-D). To further determine whether Th2 cells were decreased by SNAP, splenocytes were collected from LL2 tumor-bearing mice at Day 20 after SNAP treatment. The proportion of Th2 cells, which

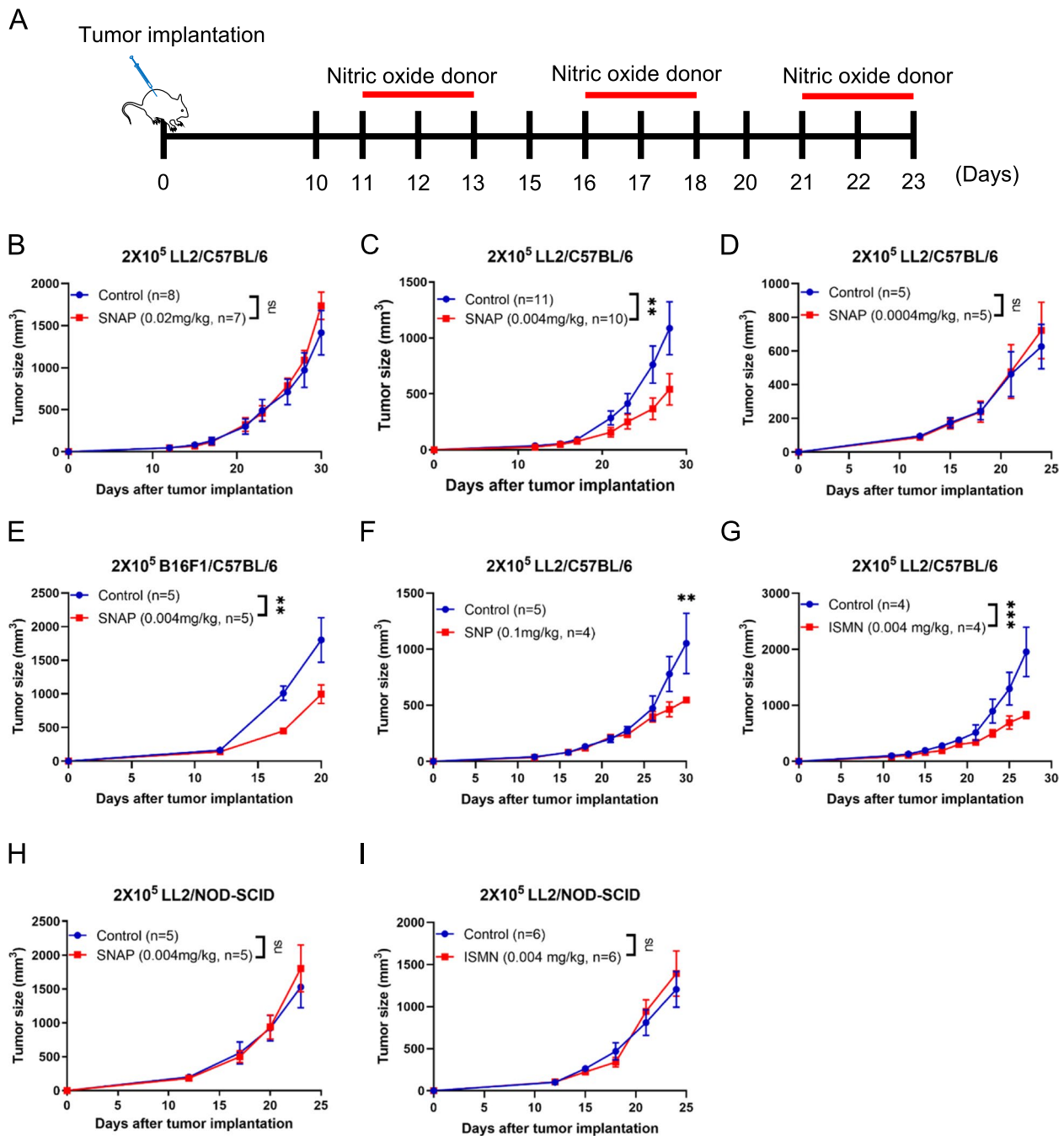


Fig. 1 Low doses of nitric oxide donors induce an antitumor response that is immune dependent. **(A)** Schematic of the tumor-bearing mouse model and the timeline of treatment with the nitric oxide donor S-nitroso-N-acetyl-DL-penicillamine (SNAP). LL2 tumor-bearing C57BL/6 mice received **(B)** 0.02, **(C)** 0.004, and **(D)** 0.0004 mg/kg SNAP. **(E)** B16F1 tumor-bearing C57BL/6 mice were administered 0.004 mg/kg SNAP by intraperitoneal injection. **(F)** LL2 tumor-bearing mice were administered SNP (0.1 mg/kg). **(G)** LL2 tumor-bearing C57BL/6 mice were administered 0.004 mg/kg isosorbide mononitrate (ISMN). **(H)** LL2 tumor-bearing immunodeficient NOD-SCID mice were administered 0.004 mg/kg SNAP or **(I)** 0.004 mg/kg ISMN by intraperitoneal injection. In all mice, 2 × 10⁵ Lewis lung carcinoma LL2 cells or B16F1 melanoma cells were implanted in the right flank. Tumor volumes were measured every 2-4 days beginning on the twelfth day after tumor implantation. The tumor results are presented as the means ± SEMs. **p* < 0.05, ***p* < 0.01, ****p* < 0.001. ns, no significant difference. All *p*-values were obtained by two-way ANOVA

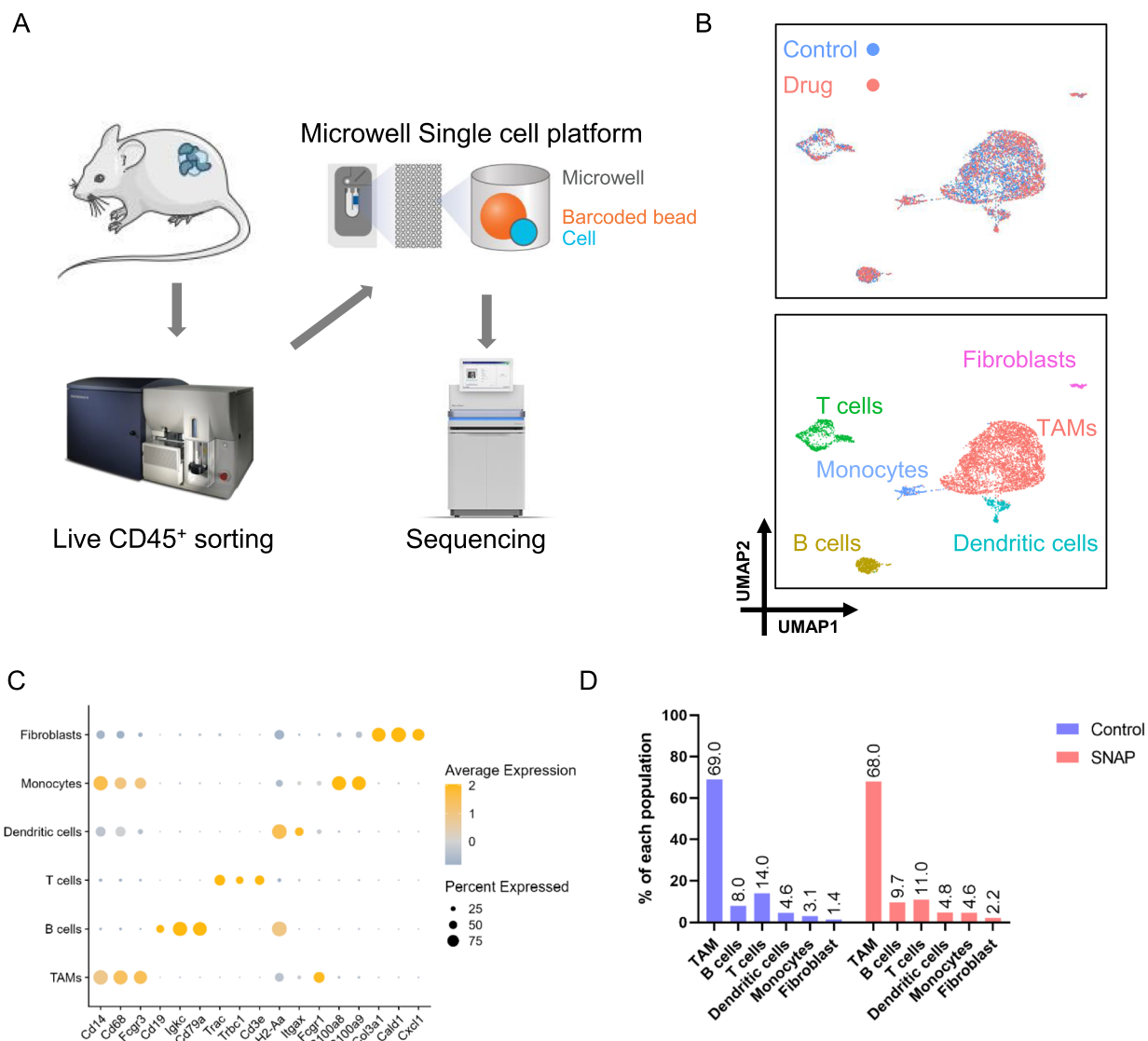


Fig. 2 The top 2 abundant infiltrating immune cells were tumor-associated macrophages and T cells. **(A)** Schematic of the study design. Single-cell RNA sequencing was used to analyze infiltrating immune cells isolated from tumor-bearing mice. **(B)** Clustering of intratumoral CD45⁺ cells and visualization of the subset. Uniform manifold approximation and projection (UMAP) of single-cell RNA sequencing data from 6563 cells (Control: 3387; Drug: 3176; upper) revealed six clusters determined by 14 specific markers (Supplementary Fig. 3). Each dot plot represents one cell. **(C)** Bubble heatmap determining the expression levels of specific marker genes in the CD45⁺ subsets and fibroblasts. **(D)** The percentages of CD45⁺ subsets and fibroblasts in the control and low-dose SNAP treatment groups

may be associated with B cells, decreased after low-dose SNAP (0.004 mg/kg) treatment (Supplementary Fig. 2 E and F). Our results suggested that low-dose SNAP (0.004 mg/kg) influenced the Th2 T-cell population, which is associated with alterations in cytokines in the spleen.

Single-cell RNA sequencing determines the landscape of the TME in response to low-dose SNAP treatment

To further understand the complex changes in immune cells in the tumor microenvironment, we used single-cell

RNA sequencing based on a microwell-based system (BD Rhapsody) to determine this profile. The changes in T cells and macrophages can be best detected by single-cell RNA sequencing given that these cell types are the most abundant immune cells in the tumor micro-environment. Tumor tissues were collected from LL2 tumor-bearing mice of the SNAP treatment group and control group and were processed into a single-cell suspension. Single-cell suspensions from three mice in each group were mixed for further analysis. Tumor-infiltrating

immune cells (CD45⁺ and 7-AAD⁻) were isolated from LL2 tumor-bearing mice of the SNAP treatment group (0.004 mg/kg) and control group (PBS containing 0.004% DMSO). CD45⁺ cells were stained with the BD sample tag, which carries a specific sequence, to identify the different groups during sequencing (Fig. 2A). A total of 9391 cells were analyzed in the two groups (4538 cells for the control group and 4853 cells for the low-dose SNAP group).

First, we classified cells into 11 clusters through clustering resolution selection (Supplementary Fig. 3 A). To identify cluster specificity, we categorized the marker genes and displayed the top five differentially expressed genes (DEGs) in each cluster (Supplementary Fig. 3 B and Supplementary Data 1). We further analyzed the gene expression intensities of 14 common markers to determine the immune cell type in these 11 clusters (Supplementary Fig. 3 C). Finally, we annotated each cluster and reduced the 11 clusters to 6 cell types (Fig. 2B) according to the intensity of the marker genes: tumor-associated macrophages (Clusters 0, 1, 2, and 3; Cd14⁺ and Cd68⁺), B cells (Cluster 4; *Igkc*⁺, and *Cd79a*⁺), T cells (Clusters 5, 8, and 9; *Cd3e*⁺ and *Trac*⁺), dendritic cells (Cluster 7; *H2-Ab1*⁺ and *Itgax*⁺), monocytes (Cluster 7; CD14⁺, *S100a8*⁺, *S100a9*⁺, and *Fcgr1*⁻) [31], and fibroblasts (Cluster 10; *Cald1*⁺ and *Col3a1*⁺). The expression levels of marker genes in the cluster were determined (Fig. 2C and Supplementary Fig. 3 D). We further analyzed the composition of CD45-positive cells between the control group and the low-dose SNAP treatment group. Tumor-associated macrophages (TAMs) were the major competent intratumoral immune cells in the two groups (69% and 68%). In addition, approximately 11-14% of cells were T cells (Fig. 2D). Our single-cell RNA sequencing results indicate that TAMs are the most abundant intratumoral immune cells. In addition, low-dose SNAP treatment did not remarkably alter the ratio of macrophage and T-cell populations in tumor microenvironments.

Low-dose SNAP treatment increases CD8⁺ T cells and natural killer (NK) cells

Given that CD8⁺ T cells are one of the key immune cells responsible for antitumor immunity, we first aimed to study the effect of low-dose SNAP treatment on the T

cell population. To efficiently identify CD4⁺ and CD8⁺ cells, we used CD4 and CD8 Ab-seq antibodies, which carry the antibody and a specific barcode for single-cell RNA analysis. To determine the populations of T cells, we subclustered the T lymphocytes that were identified by *Cd3e* and *Trac* and used uniform manifold approximation and projection (UMAP) for dimension reduction (Supplementary Fig. 4 A). A total of six clusters were identified. There were two CD8⁺ T-cell clusters: Cluster 0, central memory T cells (*Tcf7*, and *S1pr1*) and Cluster 1, CD8⁺ cytotoxic T cells (*Cd8a*, CD8 (Ab), *Gzmb*, *Nkg7*, and *Prf1*); one CD4⁺ T-cell cluster: Cluster 2, CD4⁺ regulatory T cells (CD4 (Ab), *Ctla4*, *Il2ra*); two CD3e⁺ T cells: Cluster 4, proliferating T cells (*Mki67*, *Top2a*, *Pclaf*, *Stmn1*) and Cluster 5, CD14⁺ T cells; and Cluster 3, natural killer cells (*Cd3e*, *Gzma*, *Nkg7*, *Prg1*, and *Gzmb*) (Fig. 3A and Supplementary Figure 4B and C and Supplementary Data 2). Notably, during low-dose SNAP treatment, the population of Cluster 1 CD8⁺ cytotoxic T cells (Effector T cells; T_E) increased from 21.8% to 24.2%, and Cluster 3 natural killer (NK) cells increased from 16% to 19%. In contrast, central memory T cells (T_{CM}) in Cluster 0 were significantly decreased from 36.5% to 23.9% (Fig. 3B). Analysis of the top 5 expressed genes in T_{CM} identified *Cd69* (Supplementary Data 2); therefore, *Cd69* and *Tcf7* were analyzed in 5 T cell populations and NK cells. Coexpression of *Tcf7* and *Cd69* was observed only in T_{CM} (Supplementary Fig. 5A), closely matching the exhausted T cell progenitor 1 (Tex^{prog1}) populations reported recently [32]. Additionally, biological process analysis of upregulated genes in Cluster 1 CD8⁺ cytotoxic T cells (avg_log₂FC > 0.5) indicated that several gene groups were enriched in leukocyte activation and cytotoxicity (Fig. 3C). Moreover, KEGG pathway analysis suggested that the upregulated genes were related to the NK cell-mediated immune response (e.g., *Gzmb*, *Prf1*, *Klrd1*, *Klrl1*, *Itgal*, and *Itgb2*) (Fig. 3D). To further investigate which mechanisms were altered in Cluster 1 CD8 cytotoxic T cells after low-dose SNAP treatment, 1117 DEGs derived from the low-dose SNAP group (Supplementary data 3) were used for gene set enrichment analysis (GSEA). GSEA results indicated that the DEGs of Cluster 1 CD8⁺ cytotoxic T cells exposed to low-dose SNAP treatment were enriched in negative regulation

(See figure on next page.)

Fig. 3 Low-dose SNAP increases CD8⁺ effector T cells, and the cytotoxicity pathway is enriched in these cells. **(A)** Subclustering of T lymphocytes and visualization of the subsets. Dimension reduction by UMAP displaying six subsets of T lymphocytes (814 cells). **(B)** Distribution of each subset of T lymphocytes in the control and SNAP treatment groups. **(C)** Biological process and **(D)** KEGG pathway analyses of 92 DEGs (avg_log₂-fold change > 0.5) in CD8⁺ T cells. The GeneRatio indicates the number of significant genes associated with the Gene Ontology (GO) term divided by the total number of genes in the related pathway in the database. **(E)** MSigDB ontology gene set analysis of 1117 differentially expressed genes (DEGs) in Cluster 1 CD8⁺ cytotoxic T cells after low-dose SNAP treatment; the list of DEGs is shown in the Supplementary Data. 3. DEGs were identified using the “FindMarker” function in the Seurat package. The red bar represents the upregulated pathway after low-dose SNAP treatment. All pathways were statistically significant (*p*-value < 0.05). The *p*-value of GSEA was calculated by permutation

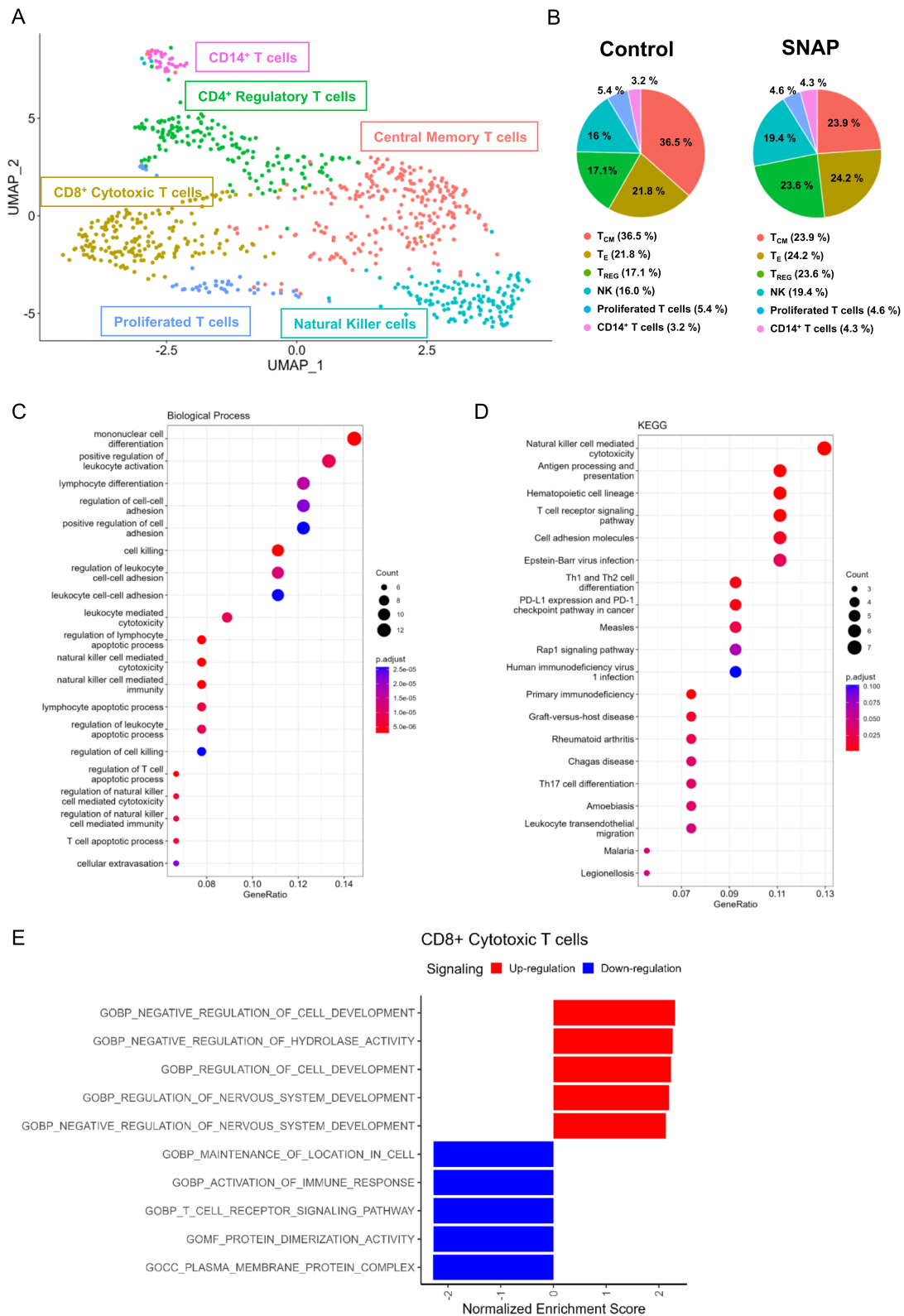


Fig. 3 (See legend on previous page.)

of hydrolase activity (Fig. 3E). GSEA results implied that hydrolase inhibition might correlate with the low-dose SNAP-induced antitumor response. Indeed, previous studies indicated that T cell activation resulted in a decrease in adipocyte triglyceride lipase, a triacylglycerol hydrolase [33]. These results suggested that low-dose SNAP increased the number of Cluster 1 CD8⁺ cytotoxic T cells and that this cluster exhibited an expression pattern associated with potentially increased cytotoxicity. GSEA results also suggest that low-dose SNAP treatment might regulate hydrolase activity to enhance T cell activation. On the other hand, GSEA analysis of 937 DEGs in NK cells indicated cluster 5 NK cells contained the interferon-gamma response gene signature (Supplementary Fig. 5B and supplementary data 4).

CD8⁺ T cell-mediated immunity is required for tumor inhibition by low-dose nitric oxide donors

Immunosuppressive cytokines, such as IL-6 and IL-10, interfere with the antitumor effects of CD8⁺ and CD4⁺ T cells in the tumor microenvironment [34, 35]. Low-dose SNAP (0.004 mg/kg) treatment decreased IL-6 and IL-10 secretion by splenocytes (Supplementary Fig. 2E). Moreover, single-cell RNA sequencing analysis indicated that low-dose SNAP treatment altered CD8⁺ T cells with activation gene signatures. Therefore, we further analyzed the percentages of CD8⁺ T cells in the tumor microenvironment after low-dose SNAP treatment using flow cytometry. Mice were treated with low-dose SNAP (0.004 mg/kg) and sacrificed on the 20th day after LL2 tumor implantation. The low-dose SNAP group exhibited smaller tumor sizes and weights than the control group (Fig. 4A). In addition, another NO donor, ISMN, also reduced tumor volume and weight upon low-dose treatment (0.004 mg/kg) (Fig. 4B). Infiltrating CD8⁺ T cells were increased by low-dose SNAP or ISMN (Fig. 4C and D). These results demonstrated that an increase in CD8⁺ T cells may play a role in the antitumor effect induced by SNAP or ISMN treatment.

To investigate the potential mechanisms by which low-dose SNAP regulates CD8⁺ T cell activation, we collected the expression profiles in the subset of T lymphocytes (Clusters 0, 1, 2, 4, and 5), excluding Cluster 3 NK cells. We further gated CD8⁺ T cells ($n = 302$) with Ab-seq antibodies (CD8 (Ab) and CD4 (Ab)) using SeqGeq software, a platform for single-cell analysis (Supplementary Fig. 6A). In addition, we selected 338 significant genes among 8369 genes in CD8⁺ T cells (average expression > 0, p value < 0.05, percentage of expressing cells > 10, SNAP/Control fold change > 1.5; Supplementary Data 5) for pathway analysis by Metacore software. Alterations in gene expression in CD8⁺ T cells were highly related to the Wnt/beta-catenin pathway (Supplementary Fig. 6B), which was recently reported to regulate CD8⁺ T-cell activation [36]. Therefore, we further isolated intratumoral CD8⁺ T cells by magnetic beads and measured the mRNA levels of beta-catenin-related genes by quantitative real-time polymerase chain reaction (RT-qPCR). Beta-catenin (Cttnb1) was significantly downregulated, and its targeted transcriptional factor 7 (Tcf7) was slightly downregulated upon treatment with low-dose SNAP (Supplementary Fig. 6C and D). In addition to the Wnt/beta-catenin pathway, cross-presentation by mature dendritic cells also contributes to CD8⁺ T cell activation [37], and the expression of C-C chemokine receptor 7 (Ccr7) in conventional dendritic cells (cDCs) plays an important role in delivering intact tumor antigen to tumor-draining lymph nodes [38] and is also a marker in the maturation of dendritic cells [39]. Single-cell RNA sequencing data revealed that *Ccr7* expression levels in dendritic cells were increased after low-dose SNAP treatment (Fig 4E). Therefore, we next examined whether low-dose SNAP increased the number of mature and activated dendritic cells in the tumor microenvironment. Flow cytometry analysis indicated that the number of cells double-positive for the dendritic cell marker CD11c and maturation marker CD86 was increased after low-dose SNAP treatment (Fig 4F). A previous study indicated that nitric oxide treatment induced immunogenic

(See figure on next page.)

Fig. 4 CD8⁺ T cells are essential for the repression of tumor growth mediated by low-dose SNAP. **(A)** Tumor tissues were isolated from LL2 tumor-bearing mice after SNAP treatment (*left*), and the tumor sizes (*middle*) and the tumor weights (*right*) were analyzed on the 20th day. **(B)** Tumor tissues were isolated from LL2 tumor-bearing mice after ISMN treatment (*left*), and the tumor sizes (*middle*) and the tumor weights (*right*) were analyzed on the 20th day. **(C)** FACS analysis of intratumoral CD8⁺ T cells between the control group and low-dose SNAP treatment group. **(D)** FACS analysis of intratumoral CD8⁺ T cells between the control group and the low-dose ISMN treatment group. The mice were sacrificed, and tumor-infiltrating lymphocytes were analyzed on the 20th day after implantation of LL2 tumor cells. **(E)** Violin plot revealing *Ccr7* expression levels in dendritic cells. Each dot represents one cell. **(F)** Flow cytometry analysis of intratumoral mature dendritic cells between the control group and low-dose SNAP treatment group. **(G)** Schematic of CD8⁺ T-cell depletion in mice (*upper*). Representative histogram of CD8⁺ expression on splenocytes (*lower*). **(H)** Simplified diagram of CD8⁺ T-cell depletion in the LL2 tumor-bearing mice (*upper*). LL2 tumor-bearing mice were treated with low-dose SNAP (0.004 mg/kg) and anti-CD8 antibody (200 μg/time) (*lower*). Anti-IgG antibody was used as the control. Both antibodies and SNAP were administered via intraperitoneal injection. The column scatter dot plot represents the mean values ± SEMs. * $p < 0.05$, ** $p < 0.01$, versus the control group. P -values of the tumor results and violin plots were obtained by two-way ANOVA and the Wilcoxon test, *** $p < 0.001$, ns, no significant difference. The tumor volumes were measured every 2 days beginning on the 10th day after tumor implantation

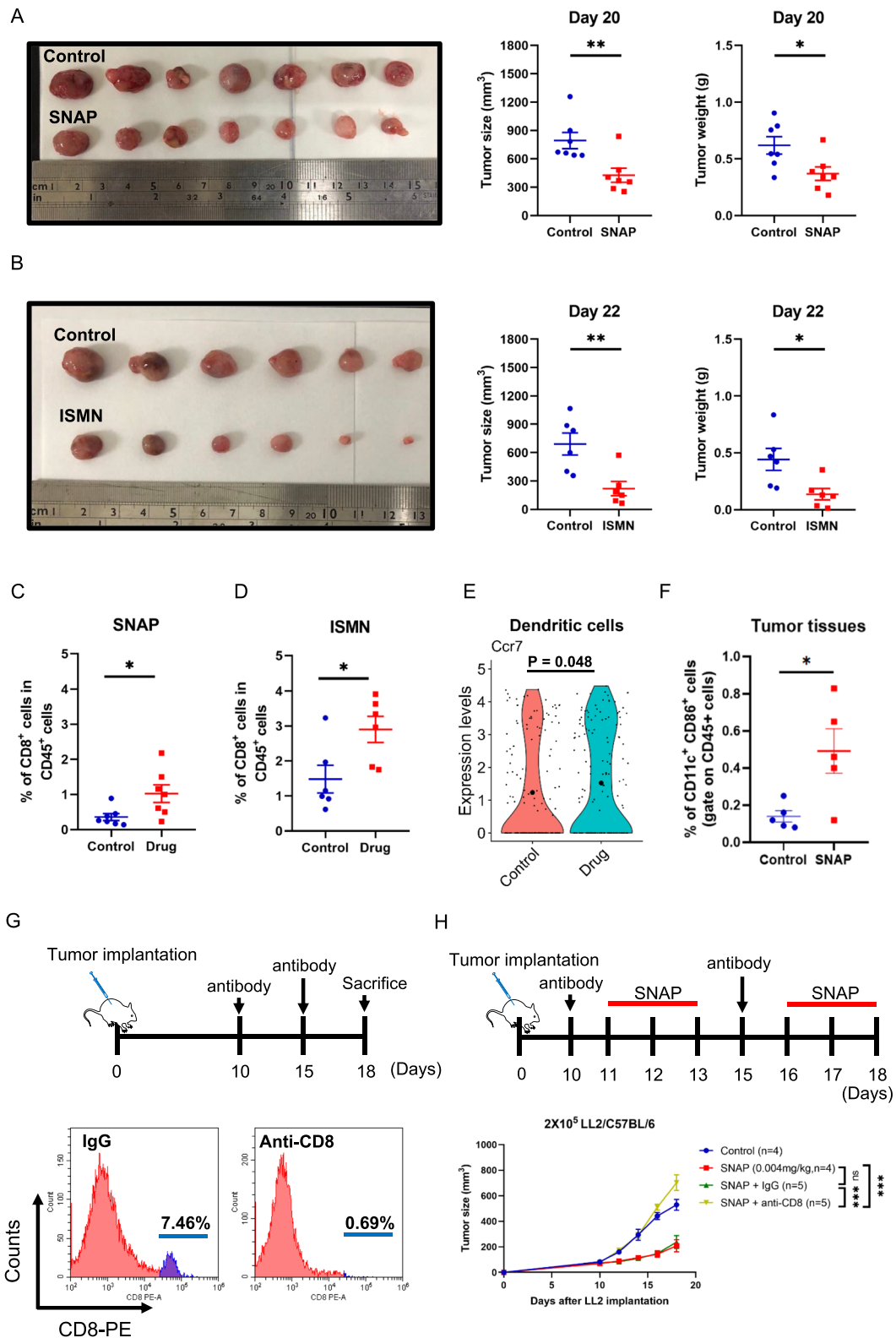


Fig. 4 (See legend on previous page.)

cell death (ICD) to control tumor progression [20]. ICD is a process in which dying cells release damage-associated molecular patterns (DAMPs) to activate the maturation of dendritic cells and induce CD8⁺ T cell activation to kill cancer cells [40]. To investigate whether the low-dose SNAP-mediated antitumor effect was correlated with ICD, we isolated tumor cells from LL2 tumor-bearing mice through CD326 magnetic beads and measured levels of the ICD marker, surface calreticulin. However, surface calreticulin was only weakly enhanced by low-dose SNAP treatment (Supplementary Fig. 7). These results demonstrated that low-dose SNAP treatment increased dendritic cell maturation and CD8⁺ T cells in the tumor microenvironment. To further determine whether CD8⁺ T cells play an essential role in the antitumor response, CD8⁺ T cells were depleted with an anti-CD8 antibody. Two doses of anti-CD8 antibody depleted approximately 90% of CD8⁺ T cells, as demonstrated by flow cytometry (Fig. 4G). The low-dose SNAP-mediated antitumor response was almost abolished by CD8⁺ T cell depletion (Fig. 4H). These results demonstrated that CD8⁺ T cells were required for the antitumor effects induced by low-dose SNAP.

The results above indicated that the low-dose SNAP-mediated antitumor response was dependent on CD8⁺ T cells and correlated with mature dendritic cells. In addition, SNAP treatment influenced the Wnt/beta-catenin pathway of CD8⁺ T cells, which may be related to CD8⁺ T-cell activation.

Low-dose SNAP increased a TAM subtype that coexpressed M1- and M2-related markers

NO is an important molecule for macrophage differentiation [41]; therefore, low-dose NO donor SNAP treatment may regulate TAM polarization. To further investigate whether low-dose SNAP treatment modulated TAM differentiation, we analyzed alterations in the expression levels of M1 and M2 macrophage markers. TAMs were subclustered into 7 clusters based on the following markers: TAM1, *Pppbp*, *Arg1*, and *Pf4*; TAM2, *Cd74*, *H2-Aa*, and *H2-Ab1*; TAM3, *C1qa*, *C1qb*, and *C1qc*; TAM4, *Il1a*, *Cxcl2*, and *Il1b*; TAM5, *Ifit47*, *Ifit3*, and *Ifit1*; TAM6, *Sell*, *Plac8*, and *Chil3*; and TAM7, *Atf3*, *Ubc*, and *Rhob* (Fig. 5A). TAM1 expressed M2 markers *Arg1* and *Mrc1*. TAM2 expressed major histocompatibility complex 2 (MHC-II) and macrophage migration inhibitory factor (MIF) receptor CD74. TAM3 expressed the complement component 1 complex genes *C1qa*, *C1qb*, and *C1qc*. TAM4 expressed the proinflammatory genes *Il1a*, *Il1b*, and *Ptgs2*. TAM5 expressed the interferon-stimulated genes *Rsad2*, *Isg15*, and *Ifit1*. TAM6 expressed *Plac8* and *Chil3*. TAM7 expressed *Klf2* and *Egr1* (Supplementary Fig. 8).

To investigate the effect of low-dose SNAP on the TAM subtype, we calculated the proportion of each TAM subset. Low-dose SNAP dramatically altered the amounts of two TAM subsets, TAM1 and TAM2 (Fig. 5B). TAM1 was increased from 18.4% to 25.4% after low-dose SNAP treatment, whereas TAM2 was decreased from 23.9% to 16.1%. Given that M1 and M2 macrophages frequently exert opposite effects on tumor progression, we analyzed M1-related genes and M2-related genes in the TAM subtypes [42–48]. TAM4 cells expressed more M1-related genes (*Ccl3*, *Nos2*, and *Il1b*), and TAM3 cells exhibited higher mRNA expression of M2-related genes (*ApoE*, *C1qa*, *C1qb*, and *C1qc*). However, TAM2 cells exhibited reduced mRNA expression levels of M1- and M2-related genes (Fig. 5C). Of note, low-dose SNAP treatment increased a particular subtype of macrophages (TAM1) that coexpressed M1- and M2-related genes, such as *Cxcl3* and *Arg1* (Fig. 5D), suggesting that low-dose SNAP regulated the inflammatory response in TAMs.

Coexpression of the M1-like gene expression signature and *Arg1* in a subpopulation of macrophages induced by SNAP

Arg1-expressing M2 macrophages in general play an immunosuppressive role through the consumption of extracellular L-arginine [49]; however, CD206-expressing M2 macrophages can be converted into cells that enhance adaptive and innate antitumor immune responses [50]. Our single-cell analysis revealed that low-dose SNAP increased the proportion of TAM1 cells that coexpressed M1- and M2-related genes (Fig. 5C). In addition, TAM1 cells did not express IL-10 (Supplementary Fig. 9), which is a key cytokine associated with immunosuppression. Therefore, it is important to further characterize the unique macrophage subpopulation induced by low-dose SNAP. We subclustered TAM1 cells, and 5 subsets were identified (TAM1-0 to TAM1-4) (Fig. 6A). The top 5 averaged genes in each subtype of TAM1 were calculated and visualized in a heatmap (Fig. 6B). TAM1-0 cells expressed *Pf4* (*Cxcl4*) and *Selenop*, which induced M2 macrophage differentiation [51], and TAM1-1 cells had high expression of heat shock protein family A members (*Hspa1a* and *Hspa1b*) and prostaglandin-endoperoxide synthase 2 (*Ptgs2*). TAM1-2 cells expressed higher levels of thrombospondin 1 (*Thbs1*). TAM1-3 cells expressed MHC-class II molecules (*H2-Eb1*, *H2-Aa*, and *H2-Ab*), and TAM1-4 cells exhibited increased prostaglandin reductase 1 (*Ptgr1*) expression. Notably, TAM1-1 cells had lower *Mrc1* (CD206) expression levels and higher expression levels of *Ptgs2*, a gene involved in the inflammatory response in M1 macrophages [52]. Low-dose SNAP treatment reduced the TAM1-0 population but increased the TAM1-1 population. On the

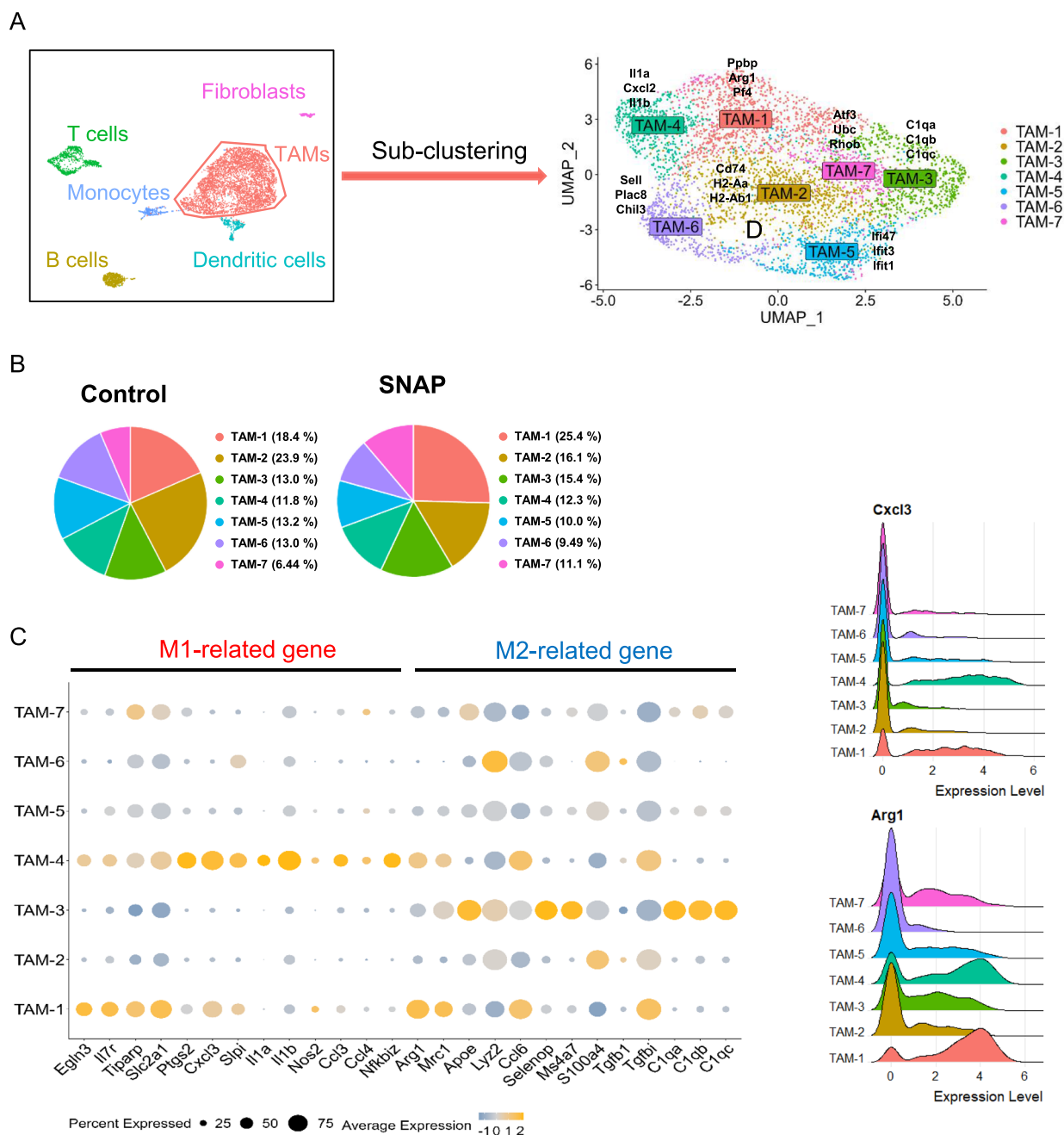


Fig. 5 Low-dose SNAP treatment induces alterations in macrophage subsets. **(A)** Subclustering of tumor-associated macrophages (TAMs) by UMAP and identifying the top three DEGs in each subset of TAMs. The top three DEGs were identified using the “FindAllMarker” function in the Seurat package. **(B)** The distribution of each TAM defined by gene expression patterns in the control or low-dose SNAP treatment groups. **(C)** The expression levels of M1-related and M2-related genes in the TAM subset. **(D)** Ridge plots determining the expression distributions of M1-related genes (Cxcl3) and M2-related genes (Arg1) in the TAM subsets. The X-axis represents log-normalized expression levels

other hand, the TAM1-2, TAM1-3, and TAM1-4 populations were not affected by SNAP (Fig. 6C). To further determine whether M1-related genes were expressed in Arg1-expressing macrophages, we analyzed M1- and M2-related genes in subsets of TAM1 cells. TAM1-0

cells expressed more M2 macrophage-related genes, and TAM1-1 cells exhibited increased expression of M1 macrophage-related genes (Fig. 6D). Indeed, flow cytometry analysis also indicated that low-dose SNAP treatment increased the population of Arg1⁺ IL7R⁺ macrophages

and Arg1⁺ CD80⁺ macrophages (Fig. 6E and F). These data suggested that low-dose SNAP treatment decreased M2-like macrophages (TAM 1-0). In addition, a unique subset of Arg1-expressing macrophages (TAM1-1) that highly expressed M1-related genes was significantly increased after low-dose SNAP treatment.

To further understand the potential roles of TAM1-0 and TAM1-1 in the tumor microenvironment, DEGs were used (800 genes in TAM1-0 cells, 991 genes in TAM1-1 cells) for hallmark gene set enrichment analysis (GSEA) (Supplementary Data 6). TAM1-0 cells had enhanced levels of coagulation and complement pathways and reduced levels of glycolysis, hypoxia, and TNF- α signaling and IFN- γ response pathways. TAM1-1 cells exhibited opposite trends based on GSEA. TAM1-1 cells displayed enrichment in proinflammatory response pathways, including TNF- α signaling, the IFN- γ response, and IL-6-JAK-STAT3 signaling (Fig. 6G). Based on GSEA, TAM1-0 cells may function as protumor macrophages; on the other hand, TAM1-1 macrophages may possess antitumor properties. Therefore, the antitumor response of low-dose SNAP was correlated with a decrease in protumor macrophages and an increase in a unique set of Arg1-positive macrophages with an antitumor gene expression signature.

Low-dose SNAP enhanced the therapeutic effect of cisplatin in tumor-bearing mouse models

Finally, combination treatment with chemotherapeutic drugs and immunomodulation agents is frequently employed in cancer patients to prolong their survival [53]. For example, immune checkpoint blockade plus cisplatin has been used to treat NSCLC [54]. Our results indicated that low-dose SNAP inhibited tumor growth via regulation of the immune system; therefore, we further tested the concept that low-dose SNAP treatment might enhance the therapeutic effect of the chemotherapeutic drug cisplatin. Mice were treated with low-dose SNAP (0.004 mg/kg) and/or cisplatin (5 mg/kg), and tumor growth was measured. The combination treatment protocol is illustrated in Fig. 7A. In the LL2 tumor-bearing mouse model, a combination of low-dose SNAP and cisplatin enhanced the cancer therapeutic effect

and prolonged survival compared with cisplatin or low-dose SNAP alone (Fig. 7B and C). Similarly, a low dose of SNP, another nitric oxide donor, enhanced the therapeutic effect and extended the survival of tumor-bearing mice (Fig. 7D and E). To further investigate whether the effective combination therapy effect can be observed in another mouse strain, BALB/C mice were implanted with CT26 colon tumor cells and treated with the same doses of SNAP, cisplatin, or both. Increased antitumor effects were observed in the CT26 tumor-bearing mouse model upon combination treatment with low-dose SNAP and cisplatin (Fig. 7F). These results indicated that low-dose SNAP enhanced the antitumor efficacy of a common chemotherapeutic drug, cisplatin. To investigate the potential mechanism responsible for the enhancement of therapeutic effects in the combination study, we performed single-cell RNA sequencing on live tumor-infiltrating immune cells from four groups (control, low-dose SNAP, cisplatin, and combination). A total of 6 clusters (TAMs, monocytes, dendritic cells, B cells, T cells and fibroblasts) were identified based on DEGs and 14 common markers (Supplementary Fig. 10A and B). T cells and NK cells were clustered into 5 clusters based on DEGs: CD3⁺ CD4⁻ CD8⁻ double negative T cells, CD4 regulatory T cells (*Cd4*, *Il2ra*, and *Foxp3*), CD8 cytotoxic T cells (*Cd8*, *Gzmb*, and *Ifng*), proliferating T cells (*Mki67*, *Top2a*, and *Pclaf*), and NK cells (*Cd3e* negative, *Klrk1*, *Nkg7*, and *Gzma*), and alterations in these clusters were assessed among the four groups of mice (Supplementary Fig. 10C). Combination treatment with low-dose SNAP and cisplatin increased the number of NK-annotated cells based on gene expression patterns. Similar percentages of CD8⁺ cytotoxic T cells were observed between the cisplatin group and the combination group. However, interestingly, combination treatment inhibited the androgen response in CD8⁺ cytotoxic T cells in GSEA (Supplementary Fig. 10D), which may inhibit CD8⁺ T-cell function [55]. These results demonstrated that an increase in NK cells is associated with an enhanced therapeutic effect in combination treatment. Additionally, the additive effect of combination treatment might correlate with the downregulation of the androgen response in CD8⁺ T cells.

(See figure on next page.)

Fig. 6 Low-dose SNAP induces a subset of macrophages displaying an M1-related gene expression signature and Arg1 expression. **(A)** Subclustering of TAM1 (978 cells) and visualization of the subsets. UMAP embedding of single-cell RNA sequencing data revealed five clusters using the “FindCluster” function. Each dot represents one cell. **(B)** Average expression levels of the top 5 DEGs in each subset of TAM1 cells. **(C)** Distribution of each TAM1 subset in the control and SNAP treatment groups. **(D)** Bubble heatmap showing the expression levels of M1-related genes and M2-related genes in the subset of TAM1 cells. **(E)** Flow cytometry analysis of intratumoral TAM1-1 cells and **(F)** CD80⁺ Arg1⁺ macrophages between the control and low-dose SNAP treatment groups. **(G)** MSigDB hallmark gene set enrichment assay (GSEA) analysis of DEGs in the TAM1-0 (*left*) and TAM1-1 (*right*) clusters. TAM1-0 and TAM1-1 DEGs were determined using the “FindMarker” function in the Seurat package and are displayed in Supplementary Data 6. All pathways were significant (p -value < 0.05). Tumor tissues were collected Day 20 after tumor implantation and used for flow cytometry analysis

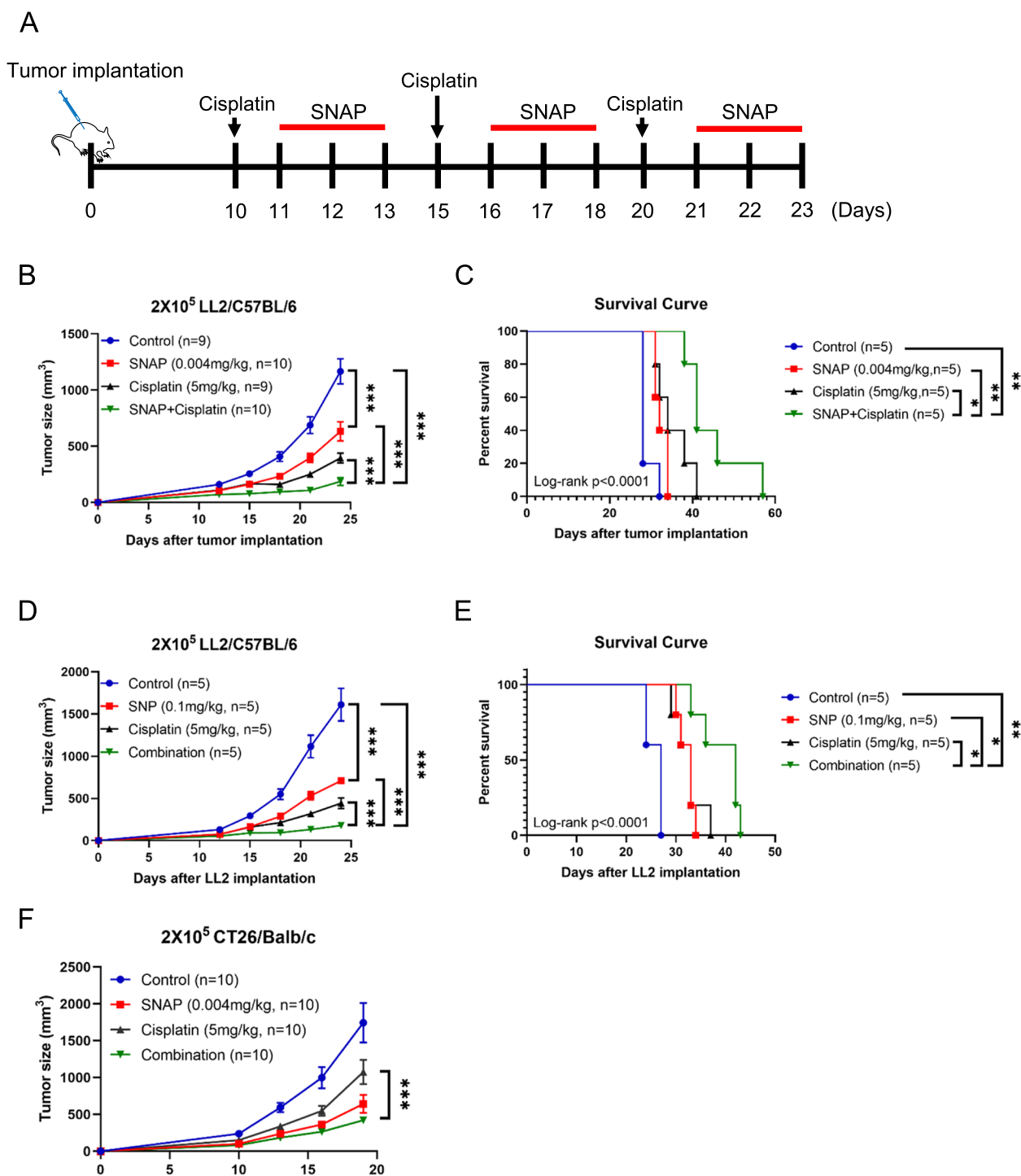


Fig. 7 Combination of nitric oxide donors and cisplatin induces an additive therapeutic effect in vivo. **(A)** Schematic representation of the combination treatment schedule of cisplatin and SNAP. **(B)** LL2 tumor-bearing mice were administered cisplatin (5 mg/kg), SNAP (0.004 mg/kg) or both, and tumor growth was measured. **(C)** The Kaplan–Meier survival curve of mice administered combination treatment with low-dose SNAP and cisplatin. **(D)** LL2 tumor-bearing mice were administered cisplatin (5 mg/kg), SNP (0.1 mg/kg) or both, and tumor growth was measured. **(E)** The Kaplan–Meier survival curve of the mice administered combination treatment with low-dose SNP and cisplatin. **(F)** CT26 tumor-bearing mice were treated with cisplatin (5 mg/kg), SNAP (0.004 mg/kg) or both, and tumor growth was measured. The p -values of the tumor growth curve were obtained by two-way ANOVA, * $p < 0.05$, ** $p < 0.01$, *** $p < 0.001$. The log-rank p -values of the survival curve were obtained using the log-rank (Mantel–Cox) test. The tumor volumes were measured every 2–4 days after tumor implantation

Discussion

IN this report, we first identified a dose-dependent effect of three different nitric oxide donors on tumor progression in subcutaneous lung tumor animal models (LL2 cells in C57BL/6 mice) and orthotopic melanoma animal models (B16F10 cells in C57BL/6 mice). The antitumor effect of a low-dose nitric oxide donor was also observed in another syngeneic immunocompetent animal model (CT-26 cells in BALB/c mice).

To investigate the immune mechanism responsible for the antitumor effect of low-dose nitric oxide donors, we used three different approaches: (1) systemic splenic cytokine expression, (2) single-cell RNA sequencing of tumor microenvironment immune cells, and (3) flow cytometry analysis of immune cells. A cytokine array revealed that IL-6 and IL-10, which are important for Th2-mediated functions, were decreased by low-dose nitric oxide donors. On the other hand, IFN- γ and TNF- α levels were increased after treatment. Flow cytometry confirmed the decrease in Th2 cells. The tumor microenvironment in the LL2 mouse model consists mainly of macrophages (approximately 70%) and T cells (approximately 10%) in our single-cell RNA analysis. We first investigated whether T cells are associated with antitumor effects. Single-cell RNA sequencing revealed that low-dose nitric oxide donors increased the population of CD8⁺ cytotoxic T cells and natural killer (NK) cells but decreased central memory T cells (T_{CM}). The increase in infiltrating CD8⁺ T cells was further verified by flow cytometry. In addition, the SNAP-mediated antitumor response was decreased after depletion of CD8⁺ T cells, demonstrating the essential role of CD8⁺ T cells. Moreover, pathway analysis of CD8⁺ T cells demonstrated that low-dose SNAP treatment altered the Wnt/beta-catenin pathway, which is upstream of Tcf. This finding suggests that low-dose SNAP-regulated T-cell activation may be related to alterations in the Wnt/beta-catenin pathway. Consistent with our findings, a previous report indicated that nitric oxide-releasing derivatives of oleanolic acid inhibit Wnt/beta-catenin signaling in colon cancer [56].

Macrophages of the TME were initially clustered into seven expression types (TAM1 to TAM7) in our immune-competent mice (Fig. 5). TAM1 and TAM4 expressed M1-related genes, suggesting antitumor characteristics. However, cluster TAM1 macrophages also expressed M2-related genes, including arginase 1. Therefore, we subclustered TAM1 into 5 subclusters: TAM1-0 to TAM1-4 macrophages. Further GSEA revealed that TAM1-0 may represent M2 protumor macrophages, whereas TAM1-1 may function as M1 antitumor macrophages. The decrease in TAM1-0 macrophages and the increase in TAM1-1 macrophages may contribute to the regression of tumors by NO donors. At present, we

are unable to determine the influence of a specific subset of macrophages due to the lack of a specific antibody against the targeting population of macrophages. On the other hand, the subset of Arg1-expressing macrophages (TAM1-0) exhibited high ApoE expression. ApoE expression in M2 macrophages regulates tumor migration in gastric cancer [57]. Additionally, human *APOE* levels were elevated in pancreatic ductal adenocarcinoma and correlated with patient survival; notably, *APOE*^{-/-} mice exhibited an increase in infiltrating CD8⁺ T cells [58]. Whether this subset of Arg1-expressing macrophages plays an important role in the tumor microenvironment warrants further study in the future.

Nitric oxide-releasing drugs have been used to treat several diseases, especially cardiovascular diseases. Our results indicated that 0.004 mg/kg SNAP ($1.81 \times 10^{-6} \text{M} \times 10^{\frac{\mu\text{l}}{\text{g}}}$) treatment or the FDA-approved drug ISMN inhibited tumor progression. It has been reported that 10^{-8}M to 10^{-4}M SNAP was sufficient to induce carotid arterial relaxation [59], implying that a lower dose of SNAP exerts a physiological effect. Indeed, 0.004 mg/kg SNAP slightly decreased systolic blood pressure 5-15 min after intraperitoneal injection. Therefore, it is necessary to monitor the patient's cardiovascular function when the low-dose releasing drugs are used in treating cancer in the future (data not shown). In addition, increasing nitrite levels from 140 to 220 nM could significantly decrease blood pressure in humans [60]. Additionally, nitric oxide levels greater than 100 nM easily activate the downstream molecule soluble guanylyl cyclase (sGC) [61]. The physiological NO concentration is suggested to range from 100 pM (or below) to approximately 5 nM [62]. Altogether, the concentrations of SNAP and ISMN used in this study are probably within the physiological range.

Interestingly, higher concentrations of NO did not exhibit antitumor effects (Fig 1). Given that the roles of NO are multifaceted and dose dependent, we hypothesized that one of the important contributing factors is angiogenesis. Therefore, we investigated whether low-dose and high-dose SNAP had different effects on angiogenesis in the tumor microenvironment using CD31, an angiogenesis marker. Immunohistochemistry staining of the tumor microenvironment revealed a lower number of CD31-positive cells in the 0.004 mg/kg treatment group compared with the control group. In contrast, CD31 staining in the tumor microenvironment was not altered by 0.02 mg/kg SNAP treatment (Supplementary Fig. 11A and B). Given that angiogenesis may cause immune suppression, a decrease in angiogenesis may further contribute to immune activation induced by low-dose exogenous nitric oxide [63].

Low-dose SNAP treatment reduced the Th2 population and the cytokines IL-6 and IL-10 in splenocytes. Moreover, low-dose SNAP treatment increased the expression levels of the Th1 cytokines IFN- γ and TNF- α , suggesting that low-dose SNAP treatment not only regulated immune cells in the TME but also systemically enhanced proinflammatory cytokines. Indeed, a low dose of the nitric oxide donor NOC-18 increased the number of murine Th1 cells [64]. On the other hand, IL-6 is also secreted by Th2 cells. High IL-6 levels correlate with a worse prognosis in patients with prostate cancer [65]. These results suggest that low-dose SNAP may also regulate systemic immunity to control tumor progression, especially by maintaining the balance between Th1 and Th2 cells.

Our cytokine assay on spleen cells indicated that several cytokines were altered by nitric oxide. The altered expressions of IL-6 and IL-10 are the most prominent. On the other hand, decreases in CCL3, CCL4, and CXCL12 were also observed. CXCL12 activates CXCR4 and CXCR7 chemokine receptors, and the signal axis is dysregulated in multiple types of cancer. Targeting the CXCL12 signal axis is a promising therapy for cancer. The expression of CXCL12 was decreased by a low dose of nitric oxide, which may in part contribute to the antitumor effects observed in our animal study [66]. CCL3 (MIP-1 α) and CCL4 (MIP-1 β) are located in chromosome 17. The expression of CCL3 and CCL4 is increased in chronic lymphocytic leukemia, and can be used as biomarkers in the therapy targeting chronic lymphocytic leukemia [67, 68]. However, the role of CCL3 and CCL4 appears to exert both antitumor and pro-tumor behavior which is context dependent in solid cancers [69].

Interestingly, low-dose SNAP treatment also increased regulatory T cells. Regulatory T cells play an important role in self-tolerance. In addition, regulatory T cells also inhibit the function of effector T cells and antigen-presenting cells [70]. Anti-CTLA4 or anti-PD-1 antibodies have been reported to enhance the antitumor response through reduction of regulatory T cell activity on effector T cells. In this regard, a combination of low-dose SNAP and anti-CTLA4 antibodies may induce a syngeneic effect on tumor regression.

Recently, cocktail treatment has become a popular approach for cancer patients, especially a combination of immune therapy and chemotherapy. For example, pembrolizumab plus chemotherapy has been used to treat metastatic non-small cell lung cancer and resulted in a better prognosis than single-drug treatment [71]. Given that cisplatin is frequently used for lung cancer and melanoma chemotherapy, cisplatin was used as a proof-of-concept drug for combination treatment with nitric oxide donors. The present results demonstrated that the

combination of low-dose SNAP and cisplatin treatment exhibited a better therapeutic effect than cisplatin treatment alone.

Conclusions

In summary, low-dose SNAP treatment induced CD8⁺ T cell activation and regulated Arg1-expressing macrophages with antitumor properties in the tumor microenvironment. Additionally, low-dose SNAP treatment reduced the expression of the anti-inflammatory cytokines IL-10 and IL-6 in the spleen. Furthermore, combination low-dose SNAP and cisplatin treatment induced an additive antitumor effect. Taken together, low-dose nitric oxide donors may emerge as a promising strategy for improving cancer immunotherapy. To the best of our knowledge, this is the first study to demonstrate the antitumor effect of low-dose exogenous nitric oxide (no carrier) on the immune system. These findings might provide a new treatment strategy for cancer using nitric oxide-releasing drugs in cancer patients.

Abbreviations

DEGs	Differentially expressed genes
GSEA	Gene Set Enrichment Analysis
IFN- γ	Interferon gamma
ISMN	Isosorbide mononitrate
KEGG	Kyoto Encyclopedia of Genes and Genomes
LL2	Lewis lung carcinoma
M1	Type 1 macrophage
M2	Type 2 macrophage
NO	Nitric oxide
NSCLC	Non-small cell lung carcinoma
SNAP	S-Nitroso-N-acetyl-DL-penicillamine
SNP	Sodium nitroprusside
TAM	Tumor-associated macrophage
T _{CM}	Central memory T cells
Th1	Type 1 helper T
Th2	Type 2 helper T
TME	Tumor microenvironment
TNF- α	Tumor necrosis factor alpha
T _{REG}	Regulatory T
UMAP	Uniform manifold approximation and projection

Supplementary Information

The online version contains supplementary material available at <https://doi.org/10.1186/s13046-022-02590-0>.

Additional file 1: Supplementary Figure 1. Low-dose SNP treatment increased nitric oxide levels in vivo and induced protein nitrosylation in vitro. (A) Nitric oxide level in the serum of control or 0.1 mg/kg SNP-treated mice was determined by measuring total serum nitrite and nitrate levels. (B). Total nitrosylated protein levels in THP-1 cells were detected using anti-biotin antibody after 30 min of SNP treatment, and GAPDH levels served as the loading control in western blotting. (C) Nitrosylated Hsp90 (SNO-Hsp90) was measured by western blotting after streptavidin agarose bead collection. The column scatter dot plot represents the mean values \pm SEMs. The *p*-value was obtained by t test.

Supplementary Figure 2. Low-dose SNAP regulates cytokine expression levels and the Th2 cell population in the spleen. (A) The tumor weight and tumor size on the day mice were sacrificed. Tumor tissues were isolated from LL2 tumor-bearing mice. The mice were sacrificed on the 20th day

after LL2 tumor implantation. (B) A cytokine array was used to determine the cytokine levels in the culture medium of splenocytes, which were co-cultured with LL2 cell lysates at 37 °C for 24 hr. The splenocytes were collected from 0.004 mg/kg SNAP treated mice (*upper*) and PBS-containing 0.004 % DMSO treated mice (*lower*). (C) The coordinates of every cytokine in the array. (D) The expression levels of each cytokine in the control and low-dose SNAP treatment groups. (E) The quadrants represent the percentage of CD4⁺ and/or IL-4-positive cells. (F) The percentage of IL-4-positive cells in the CD4⁺ population (type 2 T helper cells; Th2). LL2 tumor-bearing mice were administered SNAP (0.004 mg/kg) at 11 to 13 and 16 to 18 days, and splenocytes were isolated and analyzed. The column scatter dot plot represents the mean values \pm SEMs. * p < 0.05, versus the control group. ns, no significant difference. *P*-values of the Th2 percentages were obtained by t test. **Supplementary Figure 3.** Reduction of cell clusters from 11 to 6 by the levels of marker genes expressed in CD45⁺ cells. (A) Clustering of CD45⁺ and subset visualization. UMAP dimensionality reduction of total CD45⁺ cells (6563 cells) was executed based on visualization of relevant cell clusters. All clusters were determined using the “FindCluster” function in the Seurat package. (B) Heatmap displaying the top 5 differentially expressed genes (DEGs) and mRNA levels in 11 clusters, and the top five DEGs list is presented in Supplementary Data 1. (C) Feature plot depicting single-cell gene expression of marker genes. *Cd14*, *Cd68*, and *Itgam* are marker genes for tumor-associated macrophages (TAMs). *Cd3e* and *Trac* were used for T-cell identification. *S100a8*, *S100a9* and *Fcgr1* were used to identify monocytes (monocytes did not express *Fcgr1*). Dendritic cells were identified by *Itgax* (CD11c) and *H2-Ab1* (MHC II molecule). B cells expressed the *Igkc* and *Cd79a* genes. *Cald1* and *Col3a1* were expressed on fibroblasts. (D) Violin plot showing the expression levels of each marker gene in each cluster. **Supplementary Figure 4.** T lymphocytes are distinguished into 6 clusters and identified by marker genes. (A) Subclustering of T lymphocytes and visualization of the subsets. UMAP dimensionality reduction of 813 T lymphocytes (control: 463; drug: 350) was executed based on visualization of relevant cell clusters. All clusters were determined using the “FindCluster” function in the Seurat package. (B) Heatmap displaying the top 5 DEGs and mRNA levels in six subsets of T lymphocytes, and the gene list is shown in Supplementary Data 2. (C) Feature plot showing the single-cell gene expression of marker genes. *Cd3e* represents T cells. *CD8a* (Ab) and *Cd8a* are marker genes of CD8⁺ T cells. *Gzma*, *Gzmb*, *Prf1*, and *Nkg7* were used to identify the cytotoxic function of cells. *Tcf7* is an essential marker of central memory T cells. *CD4* (Ab) was used to identify CD4⁺ T cells, and *Il2ra* (CD25) and *Ctla4* determined the regulatory function of CD4⁺ T cells. *Mki67* is a proliferation marker. **Supplementary Figure 5.** TCF7 and CD69 expression levels in T-cell subsets and GSEA analysis of NK cells. (A) Violin plot showing *Tcf7* and *Cd69* expression levels in T-cell subsets. (B) MSigDB Hallmark gene set displayed significant overlap with the DEGs of natural killer cells. The DEGs of NK cells were identified by the “FindMarker” function in the Seurat package and the DEGs list was shown in supplementary data 4. *p*-values of the violin plot were obtained by ANOVA. ** p < 0.01, *** p < 0.001, **** p < 0.0001 versus the TAM1 group. **Supplementary Figure 6.** Low-dose SNAP regulates the Wnt/ β -catenin pathway in CD8⁺ T cells. (A) T lymphocytes were identified by CD4 (Ab) and CD8 (Ab) Abseq antibodies. Q3 are designated as CD8⁺ T cells. (B) Bar chart showing the significant pathways in CD8⁺ T cells after low-dose SNAP treatment. Significant genes were selected for pathway analysis, and the gene list is shown in Supplementary Data 5 (*p*-value < 0.05, fold change > 1.5, percentages of expressed cells > 10, and the *p*-value was obtained by t test). (C) *Cttnb1* (β -catenin) and (D) *Tcf7* mRNA levels in intratumoral CD8⁺ T cells from the control and 0.004 mg/kg SNAP treatment groups as determined by RT-qPCR. The column scatter dot plot represents the mean values \pm SEMs. *p*-values of the column scatter dot plot were obtained by t test. * p < 0.05, ns, no significant difference. **Supplementary Figure 7.** Low-dose SNAP treatment did not significantly induce the expression of surface calreticulin in LL2 tumor-bearing mice. Flow cytometry analysis of surface calreticulin in CD326-positive tumor cells isolated from LL2 tumor-bearing mice between the control and 0.004 mg/kg SNAP treatment groups. The mice were sacrificed at Day 20 after LL2 cell implantation. The column scatter dot plot represents the mean values \pm SEMs. The *p*-values were

obtained by t tests. **Supplementary Figure 8.** The mRNA levels of the top 5 differentially expressed genes in the TAM subsets. Violin plot demonstrating the expression levels of the top five DEGs in each subset of TAMs. The Y-axis represents log-normalized expression levels. **Supplementary Figure 9.** TAM1 cells do not express the immunosuppressive cytokine IL-10. Ridge plots determining IL-10 expression in the TAM1 subset. The X-axis represents log-normalized expression levels. *p*-values of the violin plot were obtained using the Wilcoxon test. ns, no significant difference.

Supplementary Figure 10. Single-cell RNA sequencing analysis of combination cisplatin and low-dose SNAP treatment. (A) Feature plot demonstrating the gene expression of marker genes. *Cd14*, *Cd68*, and *Itgam* are marker genes for tumor-associated macrophages (TAMs). *Cd3e* and *Trac* were used for T-cell identification. *S100a8*, *S100a9* and *Fcgr1* were used to identify monocytes (monocytes did not express *Fcgr1*). Dendritic cells were identified by *Itgax* (CD11c) and *H2-Ab1* (MHC II molecule). B cells expressed the genes *Igkc* and *Cd79a*. *Cald1* and *Col3a1* were expressed on fibroblasts. (B) *Left panel:* Clustering of intratumoral CD45⁺ cells and visualization of each type of cell. Uniform manifold approximation and projection (UMAP) of single-cell RNA sequencing data from 6690 cells (Control: 1909; Low-dose SNAP: 1943, Cisplatin: 1474, and Drug Combination: 1364) revealed six clusters determined by 14 specific markers (Supplementary Fig. 2). *Right panel:* Subclustering of T lymphocytes and visualization of the subsets. UMAP dimensionality reduction of 403 T lymphocytes was executed based on visualization of relevant cell clusters. (C) *Upper panel:* Violin plots revealed the expression levels of the marker genes for the subset of T cells. The Y-axis represents log-normalized expression levels. *Cd3e* serve as a T-cell marker; *Foxp3*, *Il2ra*, and *Cd4* serve as CD4 regulatory T-cell markers; *Gzmb*, *Irfng*, and *Cd8a* serve as CD8 cytotoxic T-cell markers; *Mki67*, *Top2a*, and *Pclaf* serve as proliferating T-cell markers; *Klrlk*, *Nkg7*, and *Gzma* serve as NK cell markers. *Lower panel:* The percentages of each group of the subset of T cluster within total immune cells. (D) GSEA of CD8⁺ cytotoxic T cell DEGs between combination and cisplatin treatment. The red bar chart and blue bar chart show upregulated and downregulated pathways in the combination treatment group, respectively. **Supplementary Figure 11.** Treatment with 0.004 mg/kg but not 0.02 mg/kg SNAP decreased angiogenesis in the tumor microenvironment. (A) Frozen sections of 0.004 mg/kg or (B) 0.02 mg/kg SNAP-treated and control tumors from LL2 tumor-bearing mice stained with the angiogenesis marker CD31 (red). Five randomly chosen areas in each tumor sample were used to calculate the CD31⁺ area. The column scatter dot plot represents the mean values \pm SEMs. * p < 0.05, ns, no significant difference. *p*-values of the column scatter dot plot were obtained by t test.

Additional file 2. Top 5 differentially expressed genes of intratumoral CD45⁺ cells.

Additional file 3. Top 5 differentially expressed genes in T lymphocyte subsets.

Additional file 4. Cluster 1 CD8⁺ cytotoxic T cell differentially expressed genes following low-dose SNAP treatment.

Additional file 5. Differentially expressed genes and entrezgene IDs for GSEA in cluster 3 NK cells.

Additional file 6. The expression profile of CD8a (Ab)-positive cells identified by SeqGeq platform.

Additional file 7. Differentially expressed genes of TAM1-0 and TAM1-1.

Acknowledgements

Authors thank Professor Ming-Shi Chang, Chao-Liang Wu and Liang-Yi Hung (National Cheng Kung University) for providing the mouse melanoma cell lines, LL2 murine Lewis lung carcinoma cells and CT26 murine colon carcinoma cells, respectively. The authors are grateful for the support from the Core Research Laboratory, College of Medicine, National Cheng Kung University, TMU Research Center of Cancer Translational Medicine from The Featured Areas Research Center Program within the framework of the Higher Education Sprout Project by the Ministry of Education (MOE) in Taiwan. The authors truly appreciate the professional English editing by Daniel P. Chamberlin from the Office of Research and Development at Taipei Medical University. The authors

acknowledge the statistical/computational/technical support of the Clinical Data Center, Office of Data Science, Taipei Medical University, Taiwan.

Authors' contributions

C.Y.L. designed and performed the experiments. C.Y.L., G.A., and H.D.K.T. conducted the data analysis of single-cell sequencing. H.P.H., P.F.S., and P.H.C. performed the statistics and analysis of clinical data. S.J.Y., F.W.C., P.H.Y., and T.Y.W. helped the research methods. T.Y.W. and C.Y.W. handled the processing of single-cell RNA sequencing and library construction. C.Y.L. and M.D.L. organized the data and wrote the manuscript. H.P.H., C.P.C., C.Y.W., and M.D.L. supervised the study. All authors read and approved the final manuscript.

Funding

This study was funded by Ministry of Science and Technology, Taiwan (MOST 109-2320-B-038-009, and MOST 110-2320-B-006-039) to MD Lai.

Availability of data and materials

All data generated or analyzed during this study are included in this published article. Single-cell RNA sequencing data has been uploaded to GEO.

Declarations

Ethics approval and consent to participate

All animal experiments were approved by Institutional Animal Care and Use Committee (IACUC), National Cheng Kung University (IACUC number: 109268 and 110227).

Consent for publication

All authors have agreed to publish this manuscript.

Competing interests

The authors declare that they have no competing interests.

Author details

¹College of Medicine, Institute of basic medical sciences, National Cheng Kung University, Tainan, Taiwan, ROC. ²PhD Program for Cancer Molecular Biology and Drug Discovery, College of Medical Science and Technology, Taipei Medical University and Academia Sinica, Taipei, Taiwan, ROC. ³Department of Statistics, Faculty of Science and Technology, Universitas PGRI Adi Buana, Surabaya, Indonesia. ⁴Department of Microbiology and Immunology, College of Medicine, National Cheng Kung University, Tainan, Taiwan, ROC. ⁵Department of Surgery, National Cheng Kung University Hospital, College of Medicine, National Cheng Kung University, Tainan, Taiwan, ROC. ⁶Department of Statistics, National Cheng Kung University, Tainan, Taiwan, ROC. ⁷The Center for Quantitative Sciences, Clinical Medicine Research Center, National Cheng Kung University Hospital, College of Medicine, National Cheng Kung University, Tainan, Taiwan, ROC. ⁸Department of Biochemistry and Molecular Biology, College of Medicine, National Cheng Kung University, Tainan, Taiwan, ROC. ⁹TMU Research Center of Cancer Translational Medicine, Taipei Medical University, Taipei, Taiwan. ¹⁰Graduate Institute of Cancer Biology and Drug Discovery, College of Medical Science and Technology, Taipei Medical University, Taipei, Taiwan.

Received: 25 July 2022 Accepted: 29 December 2022

Published online: 14 January 2023

References

- Hanahan D, Weinberg RA. Hallmarks of cancer: the next generation. *Cell*. 2011;144:646–74.
- Galli F, et al. Relevance of immune cell and tumor microenvironment imaging in the new era of immunotherapy. *J Exp Clin Cancer Res*. 2020;39:89.
- Mantovani A, et al. Tumour-associated macrophages as treatment targets in oncology. *Nat Rev Clin Oncol*. 2017;14:399–416.
- Gonzalez H, Hagerling C, Werb Z. Roles of the immune system in cancer: from tumor initiation to metastatic progression. *Genes Dev*. 2018;32:1267–84.
- Raskov H, et al. Cytotoxic CD8+ T cells in cancer and cancer immunotherapy. *Br J Cancer*. 2021;124:359–67.
- Thommen DS, Schumacher TN. T cell dysfunction in cancer. *Cancer Cell*. 2018;33:547–62.
- Binnewies M, et al. Understanding the tumor immune microenvironment (TIME) for effective therapy. *Nat Med*. 2018;24:541–50.
- Bult H, et al. Nitric oxide as an inhibitory non-adrenergic non-cholinergic neurotransmitter. *Nature*. 1990;345:346–7.
- Schuman EM, Madison DV. A requirement for the intercellular messenger nitric oxide in long-term potentiation. *Science*. 1991;254:1503–6.
- Wu F, et al. Single cell transcriptomics reveals lineage trajectory of retinal ganglion cells in wild-type and Atoh7-null retinas. *Nat Commun*. 2021;12:1–20.
- Forstermann U, et al. Stimulation of soluble guanylate cyclase by an acetylcholine-induced endothelium-derived factor from rabbit and canine arteries. *Circ Res*. 1986;58:531–8.
- Hottinger DG, et al. Sodium nitroprusside in 2014: A clinical concepts review. *J Anaesth Clin Pharm*. 2014;30:462–71.
- Nguyen T, et al. DNA damage and mutation in human cells exposed to nitric oxide in vitro. *Proc Natl Acad Sci U S A*. 1992;89:3030–4.
- Waldow T, et al. Nitric oxide donor-induced persistent inhibition of cell adhesion protein expression and NFκB activation in endothelial cells. *Nitric Oxide*. 2006;15:103–13.
- Sektioglu IM, et al. Macrophage-derived nitric oxide initiates T-cell diapedesis and tumor rejection. *Oncoimmunology*. 2016;5:e1204506.
- Chen J, et al. Suppression of T cells by myeloid-derived suppressor cells in cancer. *Hum Immunol*. 2017;78:113–9.
- Nath N, Kashfi K. Tumor associated macrophages and 'NO'. *Biochem Pharmacol*. 2020;176:113899.
- Burke AJ, et al. The yin and yang of nitric oxide in cancer progression. *Carcinogenesis*. 2013;34:503–12.
- Sung Y-C, et al. Delivery of nitric oxide with a nanocarrier promotes tumour vessel normalization and potentiates anti-cancer therapies. *Nat Nanotechnol*. 2019;14:1160–9.
- Jiang W, et al. Nitric oxide induces immunogenic cell death and potentiates cancer immunotherapy. *ACS Nano*. 2022;16:3881–94.
- Burgsd J-L, Ongini E, Del Soldato P. Nitric oxide-releasing drugs. *Ann NY Acad Sci*. 2002;962:360–71.
- Stokes GS, et al. A controlled study of the effects of isosorbide mononitrate on arterial blood pressure and pulse wave form in systolic hypertension. *J Hypertens*. 1999;17:1767–73.
- Yeh BK, et al. Sodium nitroprusside as a coronary vasodilator in man: I. Effect of intracoronary sodium nitroprusside on coronary arteries, angina pectoris, and coronary blood flow. *Am Heart J*. 1977;93:610–6.
- Boden WE, et al. Role of short-acting nitroglycerin in the management of ischemic heart disease. *Drug Des Devel Ther*. 2015;9:4793–805.
- Butler A, et al. Integrating single-cell transcriptomic data across different conditions, technologies, and species. *Nat Biotechnol*. 2018;36:411–20.
- Zhang Q, et al. Landscape and dynamics of single immune cells in hepatocellular carcinoma. *Cell*. 2019;179:829–845.e20.
- Zhang L, et al. Single-cell analyses inform mechanisms of myeloid-targeted therapies in colon cancer. *Cell*. 2020;181:442–459.e29.
- Jaffrey SR, Snyder SH. The biotin switch method for the detection of S-nitrosylated proteins. *Sci STKE*. 2001;2001:pl1.
- Martinez-Ruiz A, et al. S-nitrosylation of Hsp90 promotes the inhibition of its ATPase and endothelial nitric oxide synthase regulatory activities. *Proc Natl Acad Sci U S A*. 2005;102:8525–30.
- Hiam-Galvez KJ, Allen BM, Spitzer MH. Systemic immunity in cancer. *Nat Rev Cancer*. 2021;21:345–59.
- Pilling D, et al. Identification of markers that distinguish monocyte-derived fibrocytes from monocytes, macrophages, and fibroblasts. *PLoS One*. 2009;4:e7475–e7475.
- Beltra J-C, et al. Developmental relationships of four exhausted CD8+ T cell subsets reveals underlying transcriptional and epigenetic landscape control mechanisms. *Immunity*. 2020;52:825–841.e8.
- Patsoukis N, et al. PD-1 alters T-cell metabolic reprogramming by inhibiting glycolysis and promoting lipolysis and fatty acid oxidation. *Nat Commun*. 2015;6:6692.
- Culig Z. Cytokine imbalance in common human cancers. *Biochim Biophys Acta-Mol Cell Res*. 2011;1813:308–14.

35. Tsukamoto H, et al. Combined blockade of IL6 and PD-1/PD-L1 signaling abrogates mutual regulation of their immunosuppressive effects in the tumor microenvironment. *Cancer Res*. 2018;78:5011–22.
36. Gattinoni L, Ji Y, Restifo NP. Wnt/ β -Catenin signaling in T-cell immunity and cancer immunotherapy. *Clin Cancer Res*. 2010;16:4695–701.
37. Wang Y, et al. Dendritic cell biology and its role in tumor immunotherapy. *J Hematol Oncol*. 2020;13:107.
38. Bdtcher JP, Reis e Sousa C. The role of type 1 conventional dendritic cells in cancer immunity. *Trends Cancer*. 2018;4:784–92.
39. Wu Z, Hu T, Kaiser P. Chicken CCR6 and CCR7 are markers for immature and mature dendritic cells respectively. *Dev Comp Immunol*. 2011;35:563–7.
40. Kroemer G, et al. Immunogenic cell death in cancer therapy. *Annu Rev Immunol*. 2013;31:51–72.
41. Palmieri EM, et al. Nitric oxide orchestrates metabolic rewiring in M1 macrophages by targeting aconitase 2 and pyruvate dehydrogenase. *Nat Commun*. 2020;11:698.
42. Arlauckas SP, et al. Arg1 expression defines immunosuppressive subsets of tumor-associated macrophages. *Theranostics*. 2018;8:5842–54.
43. Liu S, et al. S100A4 enhances protumor macrophage polarization by control of PPAR- γ -dependent induction of fatty acid oxidation. *J Immunother Cancer*. 2021;9:e002548.
44. Bosschaerts T, et al. Alternatively activated myeloid cells limit pathogenicity associated with African trypanosomiasis through the IL-10 inducible gene selenoprotein P. *J Immunol*. 2008;180:6168–75.
45. Jablonski KA, et al. Novel markers to delineate murine M1 and M2 macrophages. *PLoS One*. 2015;10:e0145342.
46. Freereman AJ, et al. Metabolic reprogramming of macrophages: glucose transporter 1 (GLUT1)-mediated glucose metabolism drives a proinflammatory phenotype. *J Biol Chem*. 2014;289:7884–96.
47. Szulzewsky F, et al. Glioma-associated microglia/macrophages display an expression profile different from M1 and M2 polarization and highly express Gpnmb and Spp1. *PLoS One*. 2015;10:e0116644–e0116644.
48. Escribese MM, et al. The prolyl hydroxylase PHD3 identifies proinflammatory macrophages and its expression is regulated by Activin A. *J Immunol*. 2012;189:1946.
49. Duan Z, Luo Y. Targeting macrophages in cancer immunotherapy. *Signal Transduct Target Ther*. 2021;6:127.
50. Jaynes JM, et al. Mannose receptor (CD206) activation in tumor-associated macrophages enhances adaptive and innate antitumor immune responses. *Sci Transl Med*. 2020;12:eaax6337.
51. Barrett CW, et al. Selenoprotein P influences colitis-induced tumorigenesis by mediating stemness and oxidative damage. *J Clin Invest*. 2015;125:2646–60.
52. Tarique AA, et al. Phenotypic, functional, and plasticity features of classical and alternatively activated human macrophages. *Am J Respir Cell Mol Biol*. 2015;53:676–88.
53. Hattori Y, et al. A phase I/II study of weekly nab-paclitaxel plus cisplatin in chemotherapy-naïve patients with advanced non-small-cell lung cancer. *BMC Cancer*. 2020;20:115.
54. Paz-Ares L, et al. Pembrolizumab plus chemotherapy for squamous non-small-cell lung cancer. *N Engl J Med*. 2018;379:2040–51.
55. Guan X, et al. Androgen receptor activity in T cells limits checkpoint blockade efficacy. *Nature*. 2022;606:791–6.
56. Fu J, et al. Identification of nitric oxide-releasing derivatives of oleanolic acid as potential anti-colon cancer agents. *RSC Adv*. 2015;5:19445–54.
57. Zheng P, et al. Tumor-associated macrophages-derived exosomes promote the migration of gastric cancer cells by transfer of functional Apolipoprotein E. *Cell Death Dis*. 2018;9:434.
58. Kemp SB, et al. Apolipoprotein E promotes immune suppression in pancreatic cancer through NF- κ B-mediated production of CXCL1. *Cancer Res*. 2021;81:4305–18.
59. Yamashita T, et al. Apoptosis signal-regulating kinase-1 is involved in vascular endothelial and cardiac remodeling caused by nitric oxide deficiency. *Hypertension*. 2007;50:519–24.
60. Larsen FJ, et al. Effects of dietary nitrate on blood pressure in healthy volunteers. *N Engl J Med*. 2006;355:2792–3.
61. Ballou DP, et al. Revisiting the kinetics of nitric oxide (NO) binding to soluble guanylate cyclase: The simple NO-binding model is incorrect. *Proc Natl Acad Sci U S A*. 2002;99:12097.
62. Hall CN, Garthwaite J. What is the real physiological NO concentration in vivo? *Nitric Oxide*. 2009;21:92–103.
63. Kim HJ, Ji YR, Lee YM. Crosstalk between angiogenesis and immune regulation in the tumor microenvironment. *Arch Pharm Res*. 2022;45:401–16.
64. Niedbala W, et al. Effects of nitric oxide on the induction and differentiation of Th1 cells. *Eur J Immunol*. 1999;29:2498–505.
65. Nakashima J, et al. Serum interleukin 6 as a prognostic factor in patients with prostate cancer. *Clin Cancer Res*. 2000;6:2702–6.
66. Portella L, Bello AM, Scala S. CXCL12 signaling in the tumor microenvironment. *Adv Exp Med Biol*. 2021;1302:51–70.
67. Sivina M, et al. CCL3 (MIP-1 α) plasma levels and the risk for disease progression in chronic lymphocytic leukemia. *Blood*. 2011;117:1662–9.
68. Aslan B, et al. Pirtobrutinib inhibits wild-type and mutant Bruton's tyrosine kinase-mediated signaling in chronic lymphocytic leukemia. *Blood Cancer J*. 2022;12:80.
69. Mukaida N, Sasaki SI, Baba T. CCL4 signaling in the tumor microenvironment. *Adv Exp Med Biol*. 2020;1231:23–32.
70. Togashi Y, Shitara K, Nishikawa H. Regulatory T cells in cancer immunosuppression - implications for anticancer therapy. *Nat Rev Clin Oncol*. 2019;16:356–71.
71. Gandhi L, et al. Pembrolizumab plus chemotherapy in metastatic non-small-cell lung cancer. *N Engl J Med*. 2018;378:2078–92.

Publisher's Note

Springer Nature remains neutral with regard to jurisdictional claims in published maps and institutional affiliations.

Ready to submit your research? Choose BMC and benefit from:

- fast, convenient online submission
- thorough peer review by experienced researchers in your field
- rapid publication on acceptance
- support for research data, including large and complex data types
- gold Open Access which fosters wider collaboration and increased citations
- maximum visibility for your research: over 100M website views per year

At BMC, research is always in progress.

Learn more biomedcentral.com/submissions

